HHS Public Access

Author manuscript

Cell. Author manuscript; available in PMC 2019 May 31.

Published in final edited form as:

Cell. 2018 May 31; 173(6): 1398–1412.e22. doi:10.1016/j.cell.2018.03.068.

Promoter of lncRNA gene *PVT1* is a tumor suppressor DNA boundary element

Seung Woo Cho[1,13], **Jin Xu**[1,13], **Ruping Sun**[2,3], **Maxwell R. Mumbach**[1], **Ava C. Carter**[1], **Y. Grace Chen**[1], **Kathryn E. Yost**[1], **Jeewon Kim**[3], **Jing He**[1], **Stephanie Nevins**[1], **Suet-Feung Chin**[4], **Carlos Caldas**[4,5], **S. John Liu**[6,7], **Max Horbeck**[8,9,10,11], **Daniel A. Lim**[6,7,12], **Jonathan S. Weissman**[8,9,10,11], **Christina Curtis**[2,3], and **Howard Y. Chang**[1,14]

[1]Center for Personal Dynamic Regulomes, Stanford University, Stanford, CA, 94305, USA

[2]Departments of Medicine and Genetics, Stanford University School of Medicine, Stanford, CA, 94305, USA

[3]Stanford Cancer Institute, Stanford, CA, 94305, USA

[4]Department of Oncology and Cancer Research UK Cambridge Institute, Li Ka Shing Centre, University of Cambridge, Cambridge CB2 0RE, UK

[5]Breast Cancer Program, CRUK Cambridge Cancer Centre, Cambridge University Hospitals NHS Foundation Trust, Cambridge CB2 2QQ, UK

[6]Department of Neurological Surgery

[7]Eli and Edythe Broad Center of Regeneration Medicine and Stem Cell Research

[8]Department of Cellular and Molecular Pharmacology

[9]Howard Hughes Medical Institute

[10]California Institute for Quantitative Biomedical Research

[11]Center for RNA Systems Biology, University of California, San Francisco, CA 94143, USA

[12]San Francisco Veterans Affairs Medical Center, San Francisco, CA, USA

Summary

Correspondence: howchang@stanford.edu.
[13]These authors contributed equally
[14]Lead Contact

Author Contributions: S.W.C. and H.Y.C. conceived and designed the study. S.W.C., M.R.M., A.C.C., Y.G.C., K.E.Y., S.N. and S.J.L. performed experiments. S.W.C., J.X., M.R.M., A.C.C. and S.J.L. analyzed the sequencing data. J.K. performed the animal experiment. J.X., R.S., J.H. and C.Curtis analyzed the tumor patient data. S.-F.C. and C.Caldas provided human tumor data. S.J.L, M.H., D.A.L. and J.S.W. contributed experimental methods. S.W.C. and H.Y.C. wrote the manuscript with input from all authors and H.Y.C. supervised the project.

Declaration of Interest: The authors declare no competing interests.

Noncoding mutations in cancer genomes are frequent but challenging to interpret. *PVT1* encodes an oncogenic lncRNA, but recurrent translocations and deletions in human cancers suggest alternative mechanisms. Here we show that *PVT1* promoter has tumor suppressor function independent of *PVT1* lncRNA. CRISPR interference of *PVT1* promoter enhances breast cancer cell competition and growth *in vivo*. The promoters of *PVT1* and *MYC* oncogene, located 55 kilobases apart on chromosome 8q24, compete for engagement with four intragenic enhancers in the *PVT1* locus, thereby allowing *PVT1* promoter to regulate pause release of *MYC* transcription. *PVT1* undergoes developmentally regulated monoallelic expression, and *PVT1* promoter inhibits *MYC* expression only from the same chromosome via promoter competition. Cancer genome sequencing identifies recurrent mutations encompassing human *PVT1* promoter, and genome editing verified that *PVT1* promoter mutation promotes cancer cell growth. These results highlight regulatory sequences of lncRNA genes as potential disease-associated DNA elements.

Graphical abstract

Recurrent mutations in human cancer are found in the promotor for the lncRNA gene *PVT1* regulates, which regulate *MYC* transcription via promoter competition for a shared set of enhancers.

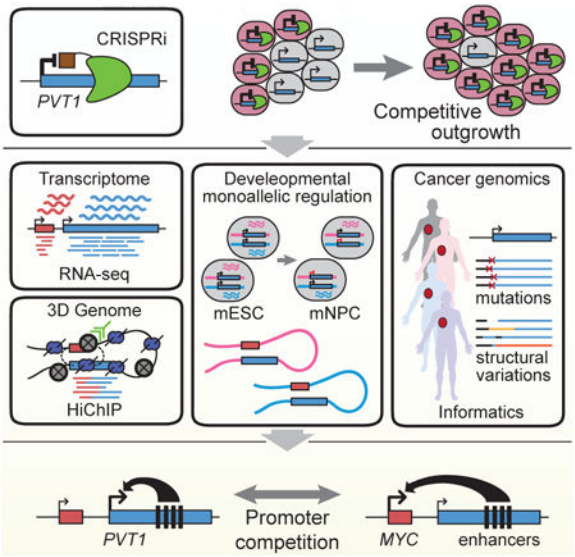

Keywords

PVT1; MYC; lncRNA; CRISPRi; topological domains; promoter; enhancer; transcriptional regulation; tumor suppressor

Introduction

The human genome encodes tens of thousands of long noncoding RNA (lncRNA) genes (Derrien et al., 2012). While some lncRNAs have emerged as central regulators of transcriptional networks in development or disease (Fatica and Bozzoni, 2014; Schmitt and Chang, 2016), the functions and regulation of most lncRNA genes are not known.

Plasmacytoma variant translocation 1 (*PVT1*) was the first lncRNA gene identified in human cancer translocations as a recurrent breakpoint in Burkitt's lymphoma (Graham and Adams, 1986; Shtivelman et al., 1989). Prior studies suggest *PVT1*-encoded lncRNA or microRNAs have oncogenic functions. The genomic region of 8q24 harboring *PVT1* is one of the most frequently amplified regions in breast cancers (Curtis et al., 2012). Indeed, PVT1 lncRNA has an oncogenic function itself by stabilizing MYC protein (Tseng et al., 2014). On the other hand, cancer genomes show recurrent structural rearrangements of *PVT1* locus that disrupt *PVT1* transcription, suggesting unknown regulatory functions of the *PVT1* locus.

In mammalian cells, each chromosome is hierarchically organized into hundreds of megabase-sized topologically associated domains (TADs) (Dixon et al., 2012). Cell type-specific enhancer-promoter contacts take place within the TAD scaffold, leading to regulated gene expression (Pombo and Dillon, 2015). Disruption of DNA boundary elements that separate neighborhoods of gene regulation has recently been recognized as an important cause of human diseases, including developmental malformations and cancer (Flavahan et al., 2016; Lupianez et al., 2015). Deletions, duplications, insertions, inversions, and translocations of genomic DNA, collectively termed structural variations, can alter the 3D chromatin conformation of the genome and cause pathogenic rewiring of enhancer-promoter contacts. *PVT1* locus harbors several intragenic enhancers that regulate transcription at target promoters by chromosome looping (Fulco et al., 2016; Zhang et al., 2016). The role of *PVT1* DNA regulatory elements in cancer is poorly understood at present.

Engineered CRISPR with transcription factor domains, called CRISPR-interference (CRISPRi) or CRISPR-activation (CRISPRa), allows control of gene expression at targeted promoters (Gilbert et al., 2013). Functional screens employing engineered transcription factors targeting random sequences in the genome were pioneered 15 years ago (Blancafort et al., 2003; Park et al., 2003), but expanding the technology to genome-wide screens for defined promoters was not feasible until recently. Recent development of CRISPRi screening technologies has enabled systematic functional studies of regulatory DNA elements and lncRNA genes in the human genome (Gilbert et al., 2014; Liu et al., 2017). We recently found that CRISPRi silencing of *PVT1* unexpectedly enhanced cell proliferation in several cell types, including two breast cancer cell lines, glioblastoma cells, and induced pluripotent stem cells (Liu et al., 2017).

Here we show that a single DNA element in the *PVT1* gene--the *PVT1* promoter--is a tumor suppressor DNA element that limits *MYC* oncogene expression. We further show that promoter competition *in cis* endows *PVT1* promoter with the function of a DNA boundary element, blocking *MYC* oncogene from accessing cell-type specific enhancers.

Results

CRISPR interference of *PVT1* enhances proliferation and cell competition

We recently established genome-scale CRISPRi to interrogate the function of lncRNA loci (Liu et al., 2017). We used single guide CRISPR RNAs (sgRNA) to direct catalytically dead Cas9 (dCas9) protein fused to KRAB repressor domain to the transcriptional start sites of lncRNA loci; each sgRNA can silence lncRNA expression in a targeted manner. The *PVT1*

locus encodes tens of annotated transcripts with at least six distinct transcriptional start sites (TSS1-6 from 5′ to 3′) (Figures 1A and S1A). The most 5′ TSS (TSS1) is located 53 kilobases (kb) downstream of the *MYC* gene, followed closely by TSS2 (+1.4 kb from TSS1). The other four TSS are scattered at ~100 kb intervals throughout the >300 kb locus, with TSS3 (+ 96.3 kb), TSS4 (+194.2 kb), TSS5 (+194.7kb), and TSS6 (+215.2 kb). Although *PVT1* has been reported as an oncogenic lncRNA, we found that CRISPRi of the *PVT1* locus surprisingly enhanced cell proliferation in multiple human cancer cell types (Liu et al., 2017) (Figure S1B). We note that it is highly unusual to observe pro-growth effect in cancer cell lines, and the pro-growth effect of *PVT1* sgRNAs was comparable to the largest effect on growth enhancement observed for silencing any protein coding gene (Gilbert et al., 2014). Among the 60 sgRNAs targeting all 6 TSS, only CRISPRi of the 5′ TSS1 or TSS2 of *PVT1* increased cancer cell proliferation (Figure S1C). CRISPRi of TSS1 was more potent than TSS2, similar results observed in both MDA-MB-231 and MCF-7 breast cancer cell lines (Figure 1B). Eight of ten different sgRNAs targeting TSS1 enhanced cell proliferation, indicating a robust and reproducible effect (Figures S1C and S1D). Therefore, we focus on TSS1 and hereafter refer to its flanking sequence as "*PVT1* promoter".

A critical element of tumor evolution is selection, wherein selectively advantageous mutations confers a fitness benefit to cells, resulting in their competitive outgrowth. In a heterogeneous population of cancer cells, individual clones grow at the expense of each other until one clone reaches dominance (Miller et al., 1988). We designed a cell competition assay to investigate the effect of noncoding genes in a heterogeneous population (Figure 1C). Notably, cells with CRISPRi-*PVT1* (mCherry+) outcompeted CRISPRi-*LacZ* control (GFP+), drastically expanded up to 75% of the total cell population within 3 passages and reached up to 85% within 10 passages. Control CRISPRi did not show any difference in growth rate with or without CRISPRi-*PVT1* in the two breast cancer cell lines (Figures 1C and S2). In 3D cell culture, CRISPRi-*PVT1* cells generated both larger colonies and many more satellite colonies with stellate morphology than control cells in the same well (Figure 1D), suggestive of an invasive phenotype (Kenny et al., 2007). These results suggest cells with CRISPRi-*PVT1* have the potential to become dominant in heterogeneous tumor population. Moreover, CRISPRi-mediated silencing of *PVT1* promoter enhanced breast tumor growth in subcutaneous xenografts *in vivo*, conferring a ~40% increase in tumor growth rate compared to control xenografts harboring a non-targeting sgRNA (p=2.1 × 10^{-3}, paired two-tailed Mann-Whitney *U*-test; Figures 1E and S1E). Because silencing *PVT1* promoter enhances cancer cell proliferation, these results demonstrate that *PVT1* promoter has an unexpected tumor suppressor function.

CRISPRi-*PVT1* increases *MYC* expression

To investigate how silencing of *PVT1* promoter enhances cell proliferation, we conducted gene expression analysis via RNA-seq. CRISPRi-*PVT1* by two independent sgRNAs each effectively reduced *PVT1* lncRNA level as expected. Interestingly, both sgRNAs yielded *MYC* mRNA as the most prominently increased RNA in the entire transcriptome (Figure 2A) without induction of differential *MYC* promoter usage or isoform switch (Figures S3A and S3B). *MYC* is a well-known oncogene requiring precise control; small quantitative

gains in *MYC* expression can promote dramatic cell competition and proliferation (Kress et al., 2015). For example, cells with 3 copies of *MYC* gene grew at the expense of cells with 2 copies of *MYC* in the developing embryo (Claveria et al., 2013). *MYC* overexpression is implicated in over 50% of human cancers, and the *MYC* gene is the adjacent chromosomal neighbor of *PVT1* promoter, making *MYC* a plausible effector gene. We observed that CRISPRi-*PVT1* also increased MYC protein level by two to three-fold, which suggests MYC protein could contribute to the pro-growth phenotype (Figure 2B).

Next, we systematically compared CRISPRi of 19 sgRNAs tiling across the *PVT1* promoter (Figures S3C and S3D, and Table S1), and investigated each sgRNA's impact on steady state *PVT1* lncRNA and *MYC* mRNA levels. CRISPRi with sgRNAs targeting downstream of *PVT1* TSS1 showed coordinately reduced *PVT1* and increased *MYC* transcript levels while sgRNAs targeting upstream of TSS1 did not alter expression of either *PVT1* or *MYC* (Figure 2C). This result suggests that silencing of *PVT1* transcription is linked with increased *MYC* expression; the lack of effect when targeting CRISPRi upstream of TSS1 also argues against potential divergent antisense transcripts from *PVT1* promoter affecting *MYC*. The ability of CRISPRi-*PVT1* to confer a competitive growth advantage was highly correlated with each sgRNA's potency to increased *MYC* mRNA level (R=0.752, Spearman's coefficient, $p=1.3 \times 10^{-4}$), more so than the level of PVT1 lncRNA silencing (R=0.658 with $p=1.5 \times 10^{-3}$) (Figure S3E). A few CRISPRi results deviated from the overall inverse trend between *PVT1* and *MYC* expression; thus elements beyond the core promoters may also be involved in this phenomenon. Furthermore, siRNA-mediated knockdown of *MYC* mRNA reverted the proliferative advantage conferred by CRISPRi-*PVT1* (Figures 2D and 2E), indicating that cell growth in *PVT1*-silenced cells requires increased *MYC* expression, similar to control cells (Figure 2F). Altogether, these results indicate *MYC* is a prominent effector of the pro-growth phenotype induced by CRISPRi-*PVT1*.

Uncoupling *PVT1* promoter vs PVT1 lncRNA in *MYC* expression and proliferation

To understand how CRISPRi-*PVT1* induces *MYC* transcription, we investigated the role of PVT1 lncRNA in *MYC* expression and the pro-growth phenotype. Three independent strategies showed that *PVT1* lncRNA is dispensable for the tumor suppressor function of *PVT1* promoter. First, we positioned dCas9 to create a transcription block and truncated the *PVT1* transcript without heterochromatin formation (Gilbert et al., 2013). dCas9-mediated interference reduced full-length PVT1 lncRNA to the same level as dCas9-KRAB, but did not increase *MYC* expression or cell proliferation (Figure 3A and S3D). Second, we transfected antisense oligonucleotide (ASO), which induce RNase H-mediated degradation of nuclear lncRNAs. ASO targeting *PVT1* reduced PVT1 lncRNA levels, but failed to increase *MYC* expression or cell growth (Figure 3B). In fact, cell viability was reduced by ASOs targeting PVT1 lncRNA, consistent with a previous study (Tseng et al., 2014). Third, siRNA-mediated knockdown through the RNA interference pathway again reduced PVT1 lncRNA levels without affecting *MYC* expression (Figure 3C). Altogether, these results suggest an lncRNA-independent mechanism by which *PVT1* promoter impacts *MYC* expression and cell growth.

Promoter competition underlies antagonism between *PVT1* and *MYC*

We identified a chromatin-based mechanism for *PVT1* regulation of *MYC* transcription. The *MYC* gene is controlled by a multitude of long-range cis-regulatory elements (Sotelo et al., 2010). Chromatin immunoprecipitation followed by deep sequencing (ChIP-seq) confirmed that dCas9-KRAB protein bound specifically to *PVT1* promoter, and induced histone H3 lysine 9 trimethylation (H3K9me3), a signature of KRAB-mediated gene repression (Liu et al., 2017), at *PVT1* promoter but not at *MYC* (Figure S4). We used HiChIP, a method for protein-directed chromosome conformation, targeting the enhancer-associated mark histone H3 lysine 27 acetylation (H3K27ac) to map the enhancer connectome in control and CRISPRi-*PVT1* cells (Mumbach et al., 2016; Mumbach et al., 2017). H3K27ac HiChIP revealed that the *PVT1* promoter and *MYC* promoter, located 58 kb apart on the linear genome, exhibit high contact frequency in 3D within a small but dense topologically associated domain (Figures 4A and S5A). Notably, four intragenic enhancers within the *PVT1* locus, herein named 822E, 866E, 912E, and 919E based on their genomic coordinates, normally contacted with *PVT1* promoter preferentially over the *MYC* locus in control cells. CRISPRi-*PVT1* decreased contacts of these four enhancers with the *PVT1* promoter but increased contacts with the *MYC* promoter and a *MYC* 3′-enhancer (Fulco et al., 2016; Figures 4A and S5B). Similar results demonstrating competitive interaction of *PVT1* intragenic enhancer between *PVT1* promoter and *MYC* 3′-enahancers were obtained in MCF-7 cells as measured by UMI-4C, an orthogonal method of targeted chromosome conformation capture with unique molecular identifiers (Schwartzman et al., 2016) (Figures 4B and S5C). These results suggest that *PVT1* promoter acts as a boundary element in breast cancer cells: *PVT1* promoter interacts with *PVT1* intragenic enhancers and blocks the latter from inducing *MYC* expression.

The *PVT1* intragenic enhancers proved to be important for *PVT1* promoter function. First, the four intragenic *PVT1* DNA elements each demonstrate bona fide enhancer activity when cloned upstream of a minimal promoter in a luciferase reporter assay (Figure S5D). Second, CRISPRi of these enhancers in MDA-MB-231 cells lowered *MYC* and *PVT1* mRNA levels, indicating that the endogenous *PVT1* enhancers regulate both genes (Figure 4C). Third and importantly, we developed a dual CRISPRi strategy to assess the function of the *PVT1* enhancers concomitant with *PVT1* promoter silencing. Dual CRISPRi of *PVT1* enhancers and *PVT1* promoter showed that silencing of 3 of 4 *PVT1* enhancers abrogated the increase in *MYC* mRNA level after *PVT1* promoter silencing (Figure 4C). Enhancer 822E is particularly intriguing because it is required for *MYC* activation only upon *PVT1* promoter silencing, but not in control cells. Together, this functional epistasis supports the idea that increased interaction between *MYC* and *PVT1* enhancers is the basis of the induction of *MYC* transcription upon silencing of *PVT1* promoter.

The model of promoter competition raises the hypothesis that *PVT1* promoter specifically inhibits *MYC* promoter firing. In metazoan genomes, RNA polymerase II (Pol II) initiates transcription for 25-60 nucleotides at most genes, and then pauses before release for productive elongation (Scruggs and Adelman, 2015). The bromodomain protein BRD4 is a key regulator of pause release, both by controlling the phosphorylation state of Pol II C-terminal domain and interaction with enhancers (Devaiah et al., 2012). *MYC* transcription is

known to be highly sensitive to the bromodomain inhibitor JQ1 (Filippakopoulos et al., 2010), and we found that JQ1 treatment similarly reduced *PVT1* transcript level, suggesting that both *MYC* and *PVT1* are regulated by bromodomain proteins (Figure S5E). Moreover, we found that CRISPRi-*PVT1* decreased BRD4 occupancy at *PVT1* promoter, but significantly increased BRD4 occupancy at *MYC* promoter as shown by ChIP-qPCR (Figure 4D). CRISPRi-*PVT1* decreased Pol II initiation at the *PVT1* locus but did not alter pol II initiation at *MYC,* as shown by serine 5-phosphorylated polymerase (Pol II-S5P) occupancy (Figure 4E). In contrast, CRISPRi-*PVT1* decreased elongating serine 2-phoshorylated RNA polymerase (pol II-S2P) at *PVT1* but increased polymerase elongation for *MYC* (Figure 4F). Moreover, interrogation of nascent transcription by 4-thiouridine (4sU) labeling (Cleary et al., 2005) showed that *PVT1* silencing decreased nascent *PVT1* transcript levels but nearly doubled *MYC* mRNA synthesis (Figure 4G). These results suggest that *PVT1* promoter is a brake for *MYC* gene transcriptional elongation.

The model of *PVT1-MYC* promoter competition also potentially explains the cell-type specificity of *PVT1* function. CRISPRi-*PVT1* did not induce *MYC* transcription in some cell types, such HCT116 colon cancer cells or HeLa cervical carcinoma cells. (Figure S5F). We found that in these cell types, *MYC* loops to the *CCAT1* enhancer instead of *PVT1* (Figures S5G to S5J); the colon cancer result is consistent with a prior study (Xiang et al., 2014). These observations provide additional evidence that the chromosome conformation landscape is an important determinant of the dynamic interplay between *PVT1* and *MYC*.

PVT1 promoter reversibly regulates *MYC* transcription

Conversely, enforced transcription from *PVT1* promoter inhibited *MYC* transcriptional elongation. We engineered MDA-MB-231 cells to stably express dCas9 fused to potent transcription activation domains (dCas9-VP64) (Konermann et al., 2015); expression of specific sgRNAs allowed us to activate transcription of endogenous loci (Figure 5A). CRISPR activation (CRISPRa) of *PVT1* increased *PVT1* lncRNA but significantly decreased *MYC* mRNA level (Figure 5B). Moreover, CRISPRa of *PVT1* reduced BRD4 occupancy at *MYC* promoter, reduced Pol II elongation at *MYC*, and reduced *MYC* nascent transcript (Figures 5C to 5F). These effects were highly specific as Pol II initiation at *MYC* was not affected. Moreover, CRISPRi-*MYC* promoter increased *PVT1* transcription (Figure 5G). These results further distinguish the RNA products as separable from the DNA element competition of the two promoters. Altogether, these results support a model of bi-directional regulation of *PVT1* and *MYC* genes via promoter competition (Figure 5H).

Monoallelic regulation of *PVT1* promoter controls *MYC* expression *in cis*

A strong prediction arising from the promoter competition model is that *PVT1* promoter should regulate *MYC* promoter on the same chromosome (i.e. the allele *in cis*). PVT1 lncRNA is known to diffuse throughout the nucleus and cytoplasm. The previously published models of PVT1 lncRNA exerting oncogenic function by interaction with RNA binding proteins or other regulatory RNAs throughout the cell predicts effect on both homologous chromosomes (i.e. action *in trans*) (Tseng et al., 2014; Wang et al., 2014a; Xu et al., 2017b). We and others recently described the recognition of wide-spread random monoallelic chromatin accessibility where one of two alleles in a diploid cell is active in a

heritable fashion (Xu et al., 2017a). Using cells derived from an F1 hybrid mouse of two highly divergent parental genome, 129S1 (here referred to as 129) and Castaneous (Cast), we isolated individual cell clones and measured chromatin accessibility, histone modifications, and RNA transcripts in an allele-specific fashion (Figure 6A). In the mouse embryonic stem cells (mESC), *Pvt1* showed bi-allelic transcription and no difference in chromatin status between two alleles. After differentiation into the neural precursor cells (mNPC), however, some clones showed monoallelic transcription of *Pvt1* (Figure 6B). A histone mark for active promoters, histone H3 lysine 4 trimethylation (H3K4me3), was observed only on the transcribed allele whereas heterochromatic H3K9me3 was only present on the silent allele at *Pvt1* promoter. Importantly, monoallelic *Pvt1* promoter activation led to specific reduction of *Myc* chromatin accessibility and mRNA level from the same chromosome, but not of the homologous chromosome in trans in the same nucleus (Figure 6B).

We found mono- or bi- allelic transcription of *Pvt1* is associated with reduction of *Myc* transcription *in cis* across numerous independent mNPC clones (Figure 6C). Based on SNPs from each allele, we calculated the allele bias of histone marks, chromatin accessibility or RNA transcription from 11 clones, represented by *d*-score. A positive or negative *d*-score indicates allelic bias towards 129 or Cast allele, respectively (Figure 6A). As expected, the *d*-score of chromatin accessibility at *Pvt1* promoter is highly correlated with the *d*-score of Pvt1 lncRNA level (R=0.990, Spearman's coefficient, $p=9.0 \times 10^{-11}$) (Figure S6A). Importantly, the *d*-score of *Pvt1* promoter chromatin accessibility is inversely correlated with the *d*-score of *Myc* mRNA level (R=-0.724 with $p=2.3 \times 10^{-3}$) (Figure 6D). Indeed, the *d*-scores of *Pvt1* and *Myc* transcript level are also inversely correlated (R=-0.733 with $p=4.4 \times 10^{-3}$) (Figure S6B). We expanded this analysis with additional independent clones via targeted reverse transcription followed by amplicon sequencing (Figure S6C). From 35 mNPC clones, the *d*-scores of *Pvt1* and *Myc* transcript levels are inversely correlated (R<-0.427 with $p<1.0 \times 10^{-2}$) whereas the control gene (*Tbp*) showed no correlation with *Pvt1* (Figures 6E and S6D). Altogether, these results indicate that *PVT1* promoter directly represses *MYC* transcription *in cis,* consistent with a DNA-element based mechanism.

Recurrent mutations encompassing *PVT1* promoter in cancer patients

Finally, somatic mutations in human cancers support a tumor suppressive role of the *PVT1* promoter. The DNA sequence of *PVT1* promoter, especially between TSS1 and TSS2, exhibits a higher degree of evolutionary conservation than other portions of the *PVT1* lncRNA, and noncoding variations in this region are predicted to be especially damaging (Figures 7A and S7A). We analyzed published cancer genomes from a variety of human tumors, and annotated the frequency of somatic mutations in the *PVT1* promoter versus mutations in other annotated lncRNA promoters on human chromosome 8. *PVT1* promoter exhibited recurrent point mutations and indels in human breast cancer and malignant lymphoma, but not other cancer types (Figure S7B). The 8q24 region spanning *MYC* and *PVT1* was recently reported to be a hotspot for somatic structural variants (SV) in breast cancer (Nik-Zainal et al., 2016). Further analysis of these data indicates that the *PVT1* promoter region is significantly enriched for SVs as compared to other lncRNA promoters (Figure 7B, *p*-value=1×10^{-5}, FDR<0.03). Human breast tumors exhibited diverse SVs,

including deletions, inversions, and duplications that overlapped the *PVT1* promoter (Figure 7C), which are expected to inactivate the tumor suppressive function of *PVT1* promoter. We also identified rare but illustrative intra-chromosomal inversion in an ER- HER2+ human breast tumor that breaks precisely in intron 1 of *PVT1,* separating *PVT1* promoter from intragenic enhancers and creating a *PVT1* fusion transcript with genes located more than 40 megabases away (Figures 7D and S7C). The chromosomal inversion and *PVT1* fusion transcripts are supported by both DNA and RNA sequencing, and is present in the majority of tumor cells, suggesting that this event occurred early or was strongly selected. *PVT1* translocations with at least 15 different fusion partners have been reported in diverse types of human cancers; these translocations invariably occur in intron 1 of *PVT1* gene, separating *PVT1* promoter from its genomic context (Chinen et al., 2014; Kim et al., 2014a; Nagoshi et al., 2012; Northcott et al., 2012; Pleasance et al., 2010; Shtivelman et al., 1989) (Table S2). These diverse translocations share the property of altering the chromatin and TAD environment of *PVT1* promoter, suggesting inactivation of repressive function of *PVT1* promoter as a unifying mechanism.

To demonstrate that mutations in *PVT1* promoter suffice to promote cell proliferation, we used CRISPR-mediated genome editing to mutate the *PVT1* promoter. After genome editing, we passaged the edited and unedited cells as a pool in a competitive growth assay. Indeed, alleles with small deletions at *PVT1* promoter were significantly enriched up to 3-fold after 10 passages, indicating that *PVT1* mutations confer a distinct growth advantage ($p<0.01$ for each allele, Figure 7E). Mutant alleles of *PVT1* promoter were further enriched longitudinally over 30 passages, suggesting their effects persist and dominate over time (Figure S7D). Further, we generated clonal MDA-MD-231 cells harboring small deletions at *PVT1*-TSS. 5 out of 6 clones showed increased *MYC* mRNA level up to 1.5-fold over cells harboring wild type *PVT1* promoter (Figures 7F and S7E). These experimental results corroborate the findings from human cancer genomes, and suggest that the *PVT1* promoter is a candidate tumor suppressor DNA element.

Discussion

Our studies may shed light on a long-standing puzzle in cancer genetics. *PVT1* was the first lncRNA gene associated with cancer, and likely also the first lncRNA associated with human disease. Frequent translocations, retroviral insertions, and interstitial deletions that disrupt the *PVT1* transcription unit have been known for more than 25 years (Shtivelman et al., 1989). In 1990, J. Michael Bishop and colleagues hypothesized that *PVT1* translocations activate *MYC* transcription (Shtivelman and Bishop, 1990), but the potential mechanism has remained obscure. Our results suggest that the *PVT1* locus harbors a series of DNA regulatory elements for *MYC*; activity of the *PVT1* promoter gates the ability of *MYC* to access these *PVT1* intragenic enhancers. Hence, the *PVT1* promoter is a tumor suppressor DNA element. Silencing *PVT1* promoter increases *MYC* transcription and cell proliferation in a manner independent of PVT1 lncRNA. Developmental monoallelic regulation of *PVT1* may also regulate somatic stem cell competition, a possibility that will be addressed elsewhere. The topography of the *MYC-PVT1* interval may underlie the tissue specificity of *PVT1* promoter action. *PVT1* promoter is located 3′ of *MYC* and regulates downstream enhancers of *MYC,* such as those active in breast cancer cells. In contrast in HeLa and

HCT116 cells where *PVT1* promoter does not regulate *MYC*, upstream *MYC* enhancers are dominant, such as the multicopy insertion of human papillomavirus sequence 500 kb upstream of *MYC* in HeLa (Adey et al., 2013) or colon cancer –specific enhancer 300 kb upstream of *MYC* in HCT116 cells (Sur et al., 2012).

A prior study using chromosome engineering in mice suggested that *PVT1* lncRNA acts as an oncogene through post-translational regulation of *MYC* protein (Tseng et al., 2014). In fact, our model is fully compatible with and may better explain the prior results. First, Tseng et al. engineered different tandem duplications of the *MYC-PVT1* interval, and found that the *MYC-PVT1* genomic DNA need to be co-amplified *in cis* to promote breast tumor growth *in vivo*. Amplification of either *MYC* or *PVT1* alone had no detectable tumorigenic activity. The cis requirement is readily explained by regulated enhancer-promoter contact in the same TAD, but difficult to explain for trans-acting lncRNA and protein products. Second, to evaluate the requirement of *PVT1* lncRNA, Tseng et al. generated a ~300 kb deletion of *PVT1* locus that also removed all four *PVT1* intragenic enhancers. This *PVT1* deletion lowered MYC level and abrogated tumorigenic activity *in vivo*, exactly as our model would predict. The recognition of *PVT1* promoter as a *MYC* transcriptional repressor suggests that *PVT1* maintains rheostatic control of *MYC* expression. The *PVT1* promoter, as a DNA element, limits *MYC* transcription while *PVT1* RNA product sustains *MYC* protein level. These two strategies of control are expected to constrain *MYC* protein level within a narrow range. The function of *PVT1* promoter is likely dominant over that of *PVT1* lncRNA as evidenced by our experimental data and the pattern of human cancer mutations. *PVT1* joins other lncRNA loci as dual DNA and RNA regulatory elements with opposing function, such as *Haunt* and *linc-p21* (Groff et al., 2016; Yin et al., 2015). Although we have shown that *PVT1* promoter inactivation enhances cell proliferation in established cancer cells, it remains to be seen whether *PVT1* promoter mutation alone can cause cancer in vivo.

Our study suggests lncRNA gene promoter as a new class of DNA boundary elements that ensure proper allocation of enhancer-promoter interactions. We posit that lncRNA promoters (and indeed any gene promoter) may serve this function due to (i) their participation in long-range 3D chromatin interactions; (ii) promoter-promoter competition to engage the same set of enhancers. *MYC* and *PVT1* transcription units do not overlap and are separated by 55 kb; hence 3D chromosome conformation is essential for promoter competition to take place. Promoter competition differs from currently known mechanisms of lncRNA-based regulation *in cis*, where transcription through the target DNA element mediates the effect (Anderson et al., 2016; Csorba et al., 2014). We show that when promoter competition is abrogated by silencing or mutation of the *PVT1* promoter, pathogenic rewiring of enhancer-promoter contact occurs between intragenic *PVT1* enhancers and the *MYC* promoter, resulting increased *MYC* expression. LncRNA promoters are more evolutionarily conserved than their gene bodies (Derrien et al., 2012), and hence this mechanism could be general. Transcriptome analyses of targeted mutations (Engreitz et al., 2016) or CRISPRi (Liu et al., 2017) of lncRNA promoters suggest approximately 10% of lncRNA promoters may regulate nearby genes by competition. 4 out of 36 lncRNA promoters silenced by CRISPRi (Liu et al., 2017) consequently activated genes within a 1 megabase window, which possibly under promoter competition or other 3D conformation-mediated regulation (Figure S7F). The advent of powerful technologies to edit the genome, epigenome, and map enhancer

connectomes now permits systematic testing of these concepts. We note that even from a DNA-centric viewpoint, the lncRNA transcript is hardly an irrelevant molecule, but is the evidence of successful competition of the lncRNA promoter at the expense of target gene promoters. With the precise mapping of tens of thousands of precise lncRNA promoters in the human genome (Hon et al., 2017), future investigations using strategies reported herein will likely illuminate novel function of lncRNA loci in cancer and other disease states.

Star Method

KEY RESOURCES TABLE is provided as a separated file.

Contact for Reagent and Resource Sharing

Further information and requests for reagents should be directed to and will be fulfilled by the Lead Contact, Howard Y. Chang (howchang@stanford.edu)

Experimental Model and Subject Details

Cell lines—MDA-MB-231, MCF-7, HEK293, HEK293T and HeLa cells were maintained with DMEM (Thermo Fisher, Cat#11995) supplemented with 10% fetal bovine serum (GE Healthcare, Cat#SH30396.03) and 1% pen-strep (Thermo Fisher, Cat#15140). SKBR3 and HCT116 cells were maintained with modified McCoy's 5A (Thermo Fisher, Cat#16600) supplemented with 10% fetal bovine serum and 1% pen-strep. MCF-10A cells were maintained with DMEM:F12(1:1) (Thermo Fisher, Cat#11320) supplemented with 5% horse serum (Thermo Fisher, Cat#16050122), 10 mg/ml insulin (Sigma Aldrich, Cat#I0516), 20 ng/ml epidermal growth factor (Thermo Fisher, Cat#PHG0311), 100 ng/ml cholera toxin (Sigma Aldrich, Cat#C8052), 0.5 μg/ml hydrocortisone (Sigma Aldrich, Cat#H0888) and 1% pen-strep. mESCs were cultured in serum (Fisher Scientific, SH30071.03) and LIF-containing (EMD Millipore, Cat#ESG1107) media on 0.2% gelatin-coated plates. mNPC cells were maintained on plates which were coated with 0.2% gelatin with N2B27 media which is composed of 1:1 mixed media of DMEM:F12(1:1) and Neurobasal media (Thermo Fisher, Cat#21103049) supplemented with 1× NDiff Neuro2 Medium Supplement (EMD Millipore, Cat#SCM012), 0.5× B-27 Supplement (Thermo Fisher, Cat#17504044), 1× Glutamax Supplement (Thermo Fisher, Cat#35050061), 0.1 mM of β-mercaptoethanol (Thermo Fisher, Cat#31350010), 10 ng/μl of epidermal growth factor (EGF, Peprotech, Cat#31509) and 10 ng/μl of fibroblast growth factor-basic (FGF, Peprotech, Cat#100-18B). In order to differentiate into mNPCs from mESC, mESCs were plated on gelatin-coated plates in N2B27 media for 7 days. On day 7, cells were dissociated with Accutase and cultured in suspension in N2B27 media supplemented with 10 ng/ml of FGF and 10 ng/ml of EGF. On day 10 cells embryoid bodies were plated onto 0.2% gelatin-coated plates and allowed to grow for 3 passages before sub-cloning single cells. For routine sub-culture, 0.25% Trypsin-EDTA (Thermo Fisher, Cat25200-114) were used for detaching of most cell lines; TrypLE Express Enzyme (Thermo Fisher, Cat#12604039) for MCF-10A or Accutase (EMD Millipore, Cat#SCR005) for mNPC. Puromycin (Thermo Fisher, Cat#A11138) was used at final concentration 1 μg/ml for all cell lines except SKBR3 (final 0.5 μg/ml) for 2 to 4 days. Blasticidin (Thermo Fisher, Cat#A1113903) was used at 4 μg/ml for MDA-MB-231, MCF-7, MCF-10A or HeLa, 2 μg/ml for HEK293 or SKBR3, or 16 μg/ml for HCT116 for 8

days. Hygromycin (Thermo Fisher, Cat#10687010) was used at 200 μg/ml for MDA-MB-231 for 8 days. All human cell lines were obtained from ATCC (American Type Culture Collection) and were tested for mycoplasma contamination.

Mouse subcutaneous xenograft—All animal experimentation was conducted according to protocols approved by the Stanford University Institutional Animal Care and Use Committee (IACUC). Six-week old female NOD.*Cg-Prkdc*^{scid} *Il2rg*^{tm1Wjl}/SzJ mice (Jackson laboratories) were housed at the animal care facility at Stanford University School of Medicine, kept under standard temperature, humidity, and timed lighting conditions and were provided with mouse chow and water ad libitum. For imaging, MDA-MB-231 cells expressing dCas9-KRAB were infected with lentivirus harboring EF1a-luciferase-2A-Hygro cassette. After hygromycin selection, luciferase activity was validated using Luciferase Reporter Assay System (Promega, Cat#E1500). Non-targeting sgRNA or sgRNA targeting *PVT1* (R2) was transduced by lentivirus infection followed by puromycin selection for 4 days. Luciferase-labeled MDA-MB-231 cell line expressing dCas9-KRAB with non-targeting sgRNA or sgRNA targeting *PVT1* was injected subcutaneously and bilaterally on the flank of the mice in 0.1 ml of sterile PBS (3×10^6 cells/animal) mixed with 50% Matrigel (BD Biosciences, Cat#356231). For bioluminescence imaging, mice received luciferin (150 mg/kg, 10 minutes prior to imaging) and were anesthetized and imaged in an IVIS 100 imaging system (Perkin Elmer). Images were analyzed with Living Image software (Perkin Elmer). Bioluminescent flux (photons/sec/cm^2/sr) was measured for the primary tumors for up to 6 weeks. J.K. performed cell injection, animal maintenance, imaging, and quantification and was blinded for the animal experiments.

Method Details

Lentivirus production and infection—For virus production, 5×10^6 or 1×10^7 of HEK293T cells were plated per 10 cm or 15 cm plate, respectively. The following day, plasmid encoding lentivirus was co-transfected with pMD2.G and psPAX2 into the cells using Lipofectamine 3000 (Thermo Fisher. Cat#L3000) or TransIT LT1 (Mirus, Cat#MIR2300) according to the manufacturer's instructions. Supernatant containing viral particles was collected 48 hours after transfection and filtered. For lentivirus encoding individual sgRNAs, virus was concentrated using Lenti-X concentrator (Clontech, Cat#631232) and stored at -80°C. Viral titer was verified by adding 10 μl to 640 μl of supernatant containing virus (1/10 for 10-fold concentrated virus) to the cells. For virus infection, virus and polybrene (final 4 mg/ml, Sigma Aldrich, Cat#107689) was added to 25% confluent cells. Fresh media was added 24 hours after infection. Media was changed with media containing appropriate antibiotics 48 hours after infection. After drug selection, cells were maintained for at least one day without drug for further experiments.

CRISPR construct—pHR-SFFV-dCas9-BFP (Addgene, Cat#46910) and pHR-SFFV-dCas9-BFP-KRAB (Addgene, Cat#46911) were used for making clonal MDA-MB-231 or MCF-7 cell lines expressing dCas9 or dCas9-KRAB. For multiple cell line experiments, dCas9-BFP-KRAB-2A-Blast construct was used which was generated by inserting 2A-Blast cassette into dCas9-BFP-KRAB vector. sgRNAs were cloned into mU6(modified)-sgRNA-Puromycin-mCherry vector, which was modified from Addgene-Cat#46914. For competitive

cell growth assay, mCherry ORF was replaced with EGFP. For CRISPR-mediated gene activation experiments, dCas9-VP64-2A-Blast (Addgene, Cat#61425) and MS2-P65-HSF1-Hygro (Addgene, Cat#61426) vectors were used and sgRNA was inserted into sgRNA2.0-puro-mCherry vector which was modified from Addgene-Cat#61427. For purifying recombinant Cas9 protein, pET28-Cas9 expression vector was generated from p3s-Cas9 (Addgene, Cat#43935). sgRNA sequences not included in CRiNCL library (Liu et al., 2017) were chosen considering number of their potential off-target sites (Cho et al., 2014). All sgRNAs used in this study are listed in Table S1.

Cell growth assay—3×10^3 cells or 1×10^5 cells were plated per 96-well or 12-well plates. For MTT assay, MTT labeling reagent (Roche, Cat#11465007001) was added and incubated at 37°C for 4 hours. Then solubilization solution was added and incubated at 37°C for overnight. Cell proliferation was measured by using spectrometer (Molecular Devices) as A550nm-A690nm. The absorbance at day 4 post plating was to the signal at day 1 post plating. For MTT assay, mean was averaged from two technical replicates. For cell counting, cells were detached 4 days post plating and counted by using Countess II FL (Thermo Fisher) with Trypan blue staining. Mean counts from triplicate measurements were used to calculate cell growth rate.

siRNA or ASO—One day before transfection, 2×10^5 cells were plated on a 12-well plate. siRNA (Qiagen) or ASO (Exiqon) was transfected into the cells using DharmaFECT4 (Dharmacon, Cat#T-2004) or Lipofectamin 2000 (Thermo Fisher, Cat#11668), respectively, with final 50 nM in 1 mL media. Media was refreshed 24 hours post transfection and cells were harvested or sub-cultured 48 hours post transfection. siRNA or ASO sequences are listed in Table S1.

qRT-PCR—RNA was prepared using RNeasy Plus mini Kit (Qiagen, Cat#74136). Purified RNA was quantified by Nanodrop (Thermo Fisher). For qRT-PCR, 60 ng of RNA and Brilliant qRT-PCR mastermix (Agilent, Cat#600825) were used. Each Ct value was measured using Lightcycler 480 (Roche) and each mean dCt was averaged from triplicate qRT-PCR reaction. Relative RNA level was calculated by ddCt method compared to *GAPDH* control. The mean dCt value of each replicate was used to calculate *p*-value. Primer sequences are listed in Table S1.

RNA-seq—50 ng of total RNA was used to RNA-seq. RNA-seq libraries were prepared using Truseq Stranded total RNA LT kit (Illumina, Cat#RS-122-2201) as according to manufacturer's instructions. Paired-end reads were obtained on HiSeq 4000. Reads were mapped by using Tophat2 (Kim et al., 2013) and analyzed by using DESeq2 (Love et al., 2014).

Western blotting—After puromycin selection, cells were harvested and lysed using RIPA buffer (50 mM Tris pH 8.0, 1mM EDTA, 150 mM NaCl, 1% Triton X-100, 0.1 % SDS, 0.1% sodium doxycholate) supplemented with cOmplete proteinase inhibitor cocktail (Roche, Cat# 11697498001). Lysate was homogenized using sonication and quantified using BCA reaction (Thermo Fisher, Cat#23227). 20 μg of lysate was resolved on NuPAGE 4-12% Bis-Tris gel (Thermo Fisher, Cat# NP0322) and transferred to nitrocellulose membrane (GE

Healthcare, Cat#10600002). After blocking using Odyssey blocking buffer-PBS (LI-COR BioSciences, Cat#927-40003), membrane was incubated for overnight at 4°C with antibody against to MYC (Cell Signaling, Cat#5605S, 1/1,000) or GAPDH (Santa Cruz, Cat#sc69778, 1/5,000). Afterward, the membrane was incubated for 1 hour at room temperature with IRDye 800CW goat anti-rabbit secondary antibody (LI-COR BioSciences, Cat#926-32211, 1/10,000) and IRDye 680RD goat anti-mouse secondary antiboby (LI-COR BioSciences, Cat#926-68070, 1/10,000). Protein bands were visualized and quantified using Odyssey CLx and Image Studio 1.0.11 (LI-COA BioSciences).

Cell growth competition assay—Cells with CRISPRi-Control or CRISPRi-*PVT1* were marked with different fluorescent proteins encoded in lentiviral vector and then co-cultured. Following puromycin selection for lentivirus infection with sgRNA, cells were counted and mixed GFP+ cells (for control sgRNA) and mCherry+ cells (for control sgRNA or sgRNA-*PVT1*). For 2D-culture, 1×10^5 cells were plated on 12-well plate and maintained by routine sub-culture every other day at 1:4 ratio and analyzed by FACSAria II (BD Biosciences). For 3D-culture, 2.5×10^5 cells in 2.5 ml of media containing 2% Matrigel were plated on 6-well plate which was coated with 450 μl of Matrigel. Media containing 2% Matrigel was refreshed at every 4 days. Fluorescence microscope images were taken by 5× magnification of Axiovert 200M (Carl Zeiss).

Northern blotting—10 mg of RNA was dissolved on a denaturing 1.2% MOPS agarose gel using formaldehyde load dye (Thermo Fisher, Cat#AM8550) followed by transferring to BrigtStar-Plus nylon membrane (Thermo Fisher, Cat#AM10104) using NorthernMax Transfer Buffer (Themo Fisher, Cat#AM8672) for overnight. RNA transferred to membrane was crosslinked by UV Stratalinker 2400 (Stratagene) with auto-crosslink protocol and baked at 80°C for 30 minutes. Membrane was incubated in ULTRAhyb-Oligo buffer (Thermo Fisher, Cat#AM8663) for 1 hour at 42°C. Then, membrane and 500 ng of denatured probe was incubated with ULTRAhyb-Oligo buffer for overnight at 55°C. After hybridization, membrane was washed twice with NorthernMax Low-Stringency Wash Solution (Thermo Fisher, Cat#AM8673) for 5 min followed by washed twice NorthernMax High-Stringency Wash Solution for 15 min at 42°C (Thermo Fisher, Cat#AM8674). Membrane was blocked using Odyssey Blocking Buffer-PBS containing 1% SDS for 1 hour at room temperature. Then, membrane was incubated with Streptavidin-IRDye 800CW (LI-COR BioSciences, Cat#926-32230, 1/10,000) in Odyssey Blocking Buffer-PBS containing 1% SDS for 30 min at room temperature followed by wash three times using PBS containing 0.1% Tween-20 for 5 min. RNA bands were visualized and quantified using Odyssey CLx and Image Studio 1.0.11. Templates of probes were amplified using reverse-transcriptase and purified on agarose gel. Then, biotin incorporated probe was generated by PCR using Hot Start Taq DNA polymerase (NEB, Cat#M0495L) and standard Taq reaction buffer (NEB, Cat#B9014S) supplemented with 125 μM of dTTP, 125 μM of biotin-16-dUTP (Roche, Cat#11093070910) and 250 μM of each dATP, dCTP and dGTP (NEB, Cat#N0446S). Probe DNA was dissolved on an 1.2% agarose gel to confirm of appropriate incorporation of biotin and purified by gel extraction. Probes were denatured prior to hybridize by incubation for 10 min at 95°C. Primer sequences used to make probes are listed in Table S1.

ATAC-seq—For ATAC-seq, 5×10^4 cells were harvested and washed by PBS. Cells were resuspended in lysis buffer (10 mM Tris-HCl pH 7.5, 10 mM $NaCl_2$, 3 mM $MgCl_2$, 0.05% NP40) and pelleted. Cell pellet was resuspended in TD buffer (10 mM Tris-HCl pH 7.5, 10 mM $MgCl_2$, 10% dimethlyformamide). 2.5 μl of Tn5 (Illumina, Cat#Fc-121-1030) was added to permeabilized cells and incubated at 37°C for 30 minutes. Fragmented DNA was purified using MinElute kit (Qiagen, Cat#28206) and library was generated by PCR using NEBnext PCR mastermix (New England Biolabs (NEB), Cat#M0541). Appropriate number of PCR cycles was determined by qPCR as described (Buenrostro et al., 2015). Libraries were sequenced on HiSeq 4000 with paired-end reads. Reads were mapped using Bowtie2 (Langmead and Salzberg, 2012) followed by removing PCR duplicates using Picard. Peaks were called using MACS2 (Zhang et al., 2008). Peaks from two biological replicates were merged using Samtools (Li et al., 2009) and Bedtools (Quinlan and Hall, 2010) and subjected to DESeq2 or calculating differences between non-targeting sgRNA or sgRNA targeting *PVT1.*

Chromatin Immunoprecipitation (ChIP)—ChIP was performed as described (Ram et al., 2011) with minor modification. Briefly, an appropriate number of MDA-MB-231 cells [2×10^6 cells for H3K27Ac (Abcam, Cat#ab4729) or H3K9me3 (Abcam, Cat#ab8898), 5×10^6 cells for Pol II-S5P (Abcam, Cat#ab5131), 1×10^7 cells for BRD4 (Bethyl Laboratories, Cat#A301-985A100), 2×10^7 cells for HA [(Cell Signaling, Cat#2367S) or Pol II-S2P (Abcam, Cat#ab5095)] or mNPC [5×10^6 cells for H3K9me3 or H3K4me3 (Active Motif, Cat#39159)] was harvested and crosslinked with 1% formaldehyde (Thermo Fisher, Cat#28908) for 10 min and subsequently quenched with final 0.125 M glycine. Chromatin was sheared using Covaris ultra sonicator to around 200 bp followed by centrifugation for clearing. Soluble fraction of sheared chromatin was diluted 5-fold with ChIP-dilution buffer (16.7 mM Tris pH 7.5, 127 mM NaCl, 1.2 mM EDTA, 1.1% Triton X-100 and 0.01% SDS) incubated with pre-mixed Dynabead of A-protein and G-protein (Thermo Fisher, #10002D or #10004D) without antibody at 4°C for 1 hour. After removing the bead, an appropriate antibody or negative control IgG was added to chromatin and incubated for overnight at 4°C. Antibody-bound chromatins were captured by incubating 2 hours with pre-mixed Dynabead of A-protein and G-protein. Chromatin- captured bead was washed twice with low-salt RIPA (50 mM Tris pH 8.0, 1 mM EDTA, 150 mM NaCl, 1% Triton X-100, 0.1% SDS and 0.1% DOC), twice with high-salt RIPA (50 mM Tris pH 8.0, 1 mM EDTA, 500 mM NaCl, 1% Triton X-100, 0.1% SDS and 0.1% DOC), twice with LiCl wash buffer (50 mM Tris pH 8.0 250 mM LiCl, 0.5% NP-40 and 0.5% DOC) and twice with TE (10 mM Tris pH 8.0 and 1 mM EDTA). Bead was resuspended in elution buffer (10 mM Tris pH 8.0, 5 mM EDTA, 300 mM NaCl and 0.5% SDS) and bead was removed by magnet. Proteinase K (NEB, Cat#P8107) was added to eluted DNA and incubated at 55°C for 2 hours followed by incubating at 65°C overnight and at 37°C for 30 minutes with RNaseA (Thermo Fisher, Cat#12091). Reverse-crosslinked DNA was purified by using MinElute column. Eluted DNA was used to qPCR or sequencing library preparation with NEBnext ultra-II kit (for human cell line, NEB, Cat#E7645) or tagmentation using Nextera enzyme (for mouse cell line). qPCR was performed using qPCR master mix (Roche, #04707516001). Each Ct value was measured using Lightcycler 480 (Roche) and each mean dCt was averaged from triplicate qPCR reaction. Ct values were normalized to relative amount of 2 to 5% of input

DNA and the mean dCt value from each replicate was used for calculating *p*-value. qPCR primers are listed in Table S1. Sequencing libraries were sequenced on HiSeq 4000 with paired-end reads. Reads were mapped by using Bowtie2 followed by removing PCR duplicates using Picard. Peaks were called using MACS2 with subtraction of input signal. Peaks from two biological replicates were merged using Samtools and Bedtools. Differences between non-targeting sgRNA or sgRNA targeting *PVT1* were analyzed by DESeq2. Enrichment of any IgG control between CRISPRi-Control and CRISPRi-*PVT1* is not significantly different ($p>0.05$).

JQ1 treatment—4×10^6 cells were plated on 6-well plate. JQ1 (Sigma Aldrich, Cat#SML1524) in DMSO was added final 1 μM or 5 μM 1 day post plating. After 6 hours, cells were harvested and RNA was extracted as decribed in qRT-PCR method. Equal volume of DMSO without JQ1 was added as a negative control.

Hi-ChIP—Hi-ChIP was performed as described (Mumbach et al., 2016). Briefly, 1×10^7 cells for each biological replicate were collected and crosslinked by using 1% formaldehyde for 10 minutes. Chromatin was digested using MboI restriction enzyme (NEB, Cat#R0147) followed by end-repair, ligation and sonication. Sheared chromatin was cleared and 3-fold diluted as described in ChIP method and then incubated with anti-H3K27ac antibody at 4°C for overnight. Chromatin-antibody complex was captured by Dynabead Protein-A bead. Biotin was incorporated by adding DIBO-biotin (Thermo Fisher, Cat#C-10412) followed by capture with Streptavidin C-1 bead (Thermo Fisher, Cat#65002). Captured DNA was quantified using Qubit (Thermo Fisher) and an appropriate amount of Tn5 enzyme was added to captured DNA to generate sequencing library. Sequencing was performed on HiSeq 4000 with paired-end read and analyzed by using HiC-pro (Servant et al., 2015).

UMI-4C—UMI-4C was performed as described (Schwartzman et al., 2016) with minor modification. 5×10^6 cells were harvested and crosslinked with 1% formaldehyde for 10 minutes. Pellet was resuspended in ice-cold lysis buffer (10 mM Tris pH 8.0, 10 mM NaCl, 0.2% NP-40) and incubated at 4°C for 30 min. Nuclei was pelleted and resuspended in 0.5% SDS followed by incubation at 62°C for 10 min. Chromatin was digested by MboI restriction enzyme and ligated by T4 DNA ligase (NEB, Cat#M0202) at room temperature for 4 hrs. Reaction was cleared by centrifugation. Pellet was resuspended in Proteinase K buffer (10 mM Tris pH. 7.5, 100 mM NaCl, 1 mM EDTA, 0.5% SDS) and incubated 55°C for 2 hours with Proteinase K and then incubated 68°C for 2 hours. After incubating with RNaseA, DNA was purified by ethanol precipitation. DNA was resolved in 10 mM Tris pH 7.5 and sonicated by Bioruptor followed by sequential incubation with end repair mix (NEB, Cat#E6050), Klenow exo- (NEB, Cat#M0212) and CIP (NEB, Cat#M0290). Reaction was cleared by SPRI selection (2×, Beckman Coulter, Cat#B23318). Illumina forked adaptors was added to DNA and incubated with Quick Ligase (NEB, Cat#M2200) at room temperature for 15 minutes. To release the non-ligated strand of the adaptor, DNA was denatured at 95°C for 2 minutes and then purified by SPRI (1×). Denatured DNA was quantified by Qubit. 200 ng of DNA was used for library preparation by nested PCR. Sequencing was performed on MiSeq or HiSeq 4000 with paired-end reads and analyzed by using HiC-pro. The interaction frequency was measured from two biological replicates each

of which comprises two technical replicates with two different primers. Mean was normalized to CRISPRi-Control for each interaction. PCR primers used in UMI-4C are listed in Table S1.

4C-Seq—Chromosome conformation capture combined with high-throughput sequencing (4C-Seq) was performed according to described (Stadhouders et al., 2013) with modifications. 5×10^6 cells were fixed by adding 37% formaldehyde to a final concentration of 1% and incubating for 10 minutes at room temperature while tumbling, followed by addition of 1M glycine to a final concentration of 0.125M to quench. Samples were washed with cold PBS and resuspended in 5 mL ice-cold lysis buffer (10 mM Tris-HCl (pH 8.0), 10 mM NaCl, 0.2% NP-40 supplied with proteinase inhibitor), followed by 10 min incubation on ice. Samples were re-resuspended in 500 μL 1.2× CutSmart restriction digest buffer (NEB). 20% SDS was added to a final concentration of 0.3%, and samples were incubated for 1 hr at 37°C while shaking at 900 rpm on a thermomixer. 20% Triton X-100 was added to a final concentration of 2%, followed by incubation for 1 hr at 37°C while shaking at 900 rpm on a thermomixer. NlaIII (NEB, #R0125) was added to each sample and incubated 20 hr at 37°C while shaking at 900 rpm on a thermomixer. To inactivate enzyme, 20% SDS was added to a final concentration of 1.6% SDS, followed by incubation for 25 min at 65°C while shaking at 900 rpm on a thermomixer. T4 DNA Ligase buffer (NEB) and T4 DNA Ligase (NEB) were added, and incubated for 18 hr at 16°C. Proteinase K (Machery Nagel, #740506) and incubating for 16 hr at 65°C. RNase was added and incubated for 30 min at 37°C. DNA was purified by phenol:chloroform extraction followed by ethanol precipitation. The second 4C-Seq digest was then performed by digestion using DpnII (NEB, #R0543) for 16 hr at 37°C. Digests were then purified using phenol:chloroform and resuspended in distillated water. Second ligation was performed by adding 10× T4 DNA Ligase buffer (NEB) and T4 DNA Ligase (NEB), followed by incubation for 18 hr at 16°C. Circularized fragments were purified by phenol:chloroform and resuspended in 10 mM Tris-HCl (pH 7.5), and then purified again using NucleoSpin PCR Clean-up (Machery Nagel, #740609). 1.2 μg of each template was amplified using the Expand Long Template PCR kit (Roche, #11681834001) for 30 cycles. PCR primers used for 4C-seq were described in Table S1. PCR amplicons were purified using Agencourt Ampure XP beads. Sequencing libraries were generated using the KAPA HyperPlus kit according to manufacturer's recommendations with modifications. 4C-Seq libraries were validated using the Agilent 2200 High Sensitivity DNA ScreenTape, Qubit, and ddPCR (Bio-Rad). Cluster generation and sequencing was performed on a HiSeq 4000 with single end read. Reads were aligned to the human genome using the spliced read aligner HISAT2 (Kim et al., 2015).

Luciferase reporter assay—Genomic region harboring *PVT1* intragenic enhancers was amplified by nested-PCR and cloned into pGL4.23[luc2/minP] vector (Promega, Cat#E8411) digeted by XhoI and HindIII using NEBuilder Hifi DNA Assembly Master Mix (NEB, Cat#E2621L). Luciferase activity was measured using Luciferase Assay System (Promega, Cat#E1500). One day prior to transfection, 1×10^5 of MDA-MB-231 cells plated in 24-well plate. 500 ng of plasmid was transfected into the cells using Lipofectamine 3000. Fresh media was replaced at post 24 hours transfection. At post 48 hours transfection, media was removed and the plate washed by PBS briefly. 200 μl of 1× Cell Culture Lysis Reagent

was added to plates directly and transferred to new tubes. After brief centrifugation, 20 μl of cell lysate was mixed with 100 μl of Luciferase Assay Reagent. Luminescence was measured using pre-set protocol of SpectraMax M5 and SoftMax Pro 6.3 software (Molecular Devices).

CRISPRi targeting enhancers—In order to target enhancer region efficiently which long around 1 kb, we used three sgRNA in one vector system (Adamson et al., 2016). In order to select cells infected both sgRNA targeting *PVT1* and enhancer, lentiviral vector backbone was modified by replacing Puromycin-mCherry cassette to Hygromycin resistance gene. Three sgRNAs were designed for each enhancer and cloned into pMJ114 (bovine U6, Addgene, Cat#85995), pMJ117 (human U6, Addgene, Cat#85997) or pMJ179 (mouse U6, Addgene, Cat#85996) individually. Then, U6 promoter and sgRNA sequences were amplified by PCR and combined into lentiviral vector using NEBuilder Hifi DNA Assembly Master Mix, which digested with XbaI and XhoI. Cells infected lentivirus containing sgRNA targeting *PVT1* or *LacZ* (control) first followed by Puromycin selection for 4 days as described above. Then, cells were re-plated by 1:8 ratio to 6 well plate and infected with lentivirus harboring three sgRNAs targeting each enhancer and selected with Hygromycin for 8 days. After one day recovery without antibiotics, RNAs were extracted and used for qRT-PCR. Sequences of sgRNAs and primers are listed in Table S1.

4sU-labeling—Nascent RNA labelling with 4sU was performed as described with minor modification (Duffy et al., 2015). 1×10^6 cells were plated on 15 cm plate 1 day prior to labelling. 4-thiouridine (Sigma Aldrich, Cat#T4509) dissolved in DMSO or equal volume of DMSO was added to media at final 200 μM and incubated at 37°C for 20 minutes. After incubation, cells were harvested and stored at -80°C for overnight. Total RNA was purified by adding TRIzol (Thermo Fisher, Cat#15596018) and 0.2 volume of chloroform. 1 volume of ethanol was added to aqueous phase and then transferred to RNeasy midi column (Qiagen, Cat#75144). RNA was eluted in RNase free water and quantified by Nanodrop. 5 μg of MTSEA biotin-XX (Biotium, Cat#90066) was added to 20 μg of RNA and then incubated for 2 hours in final 400 μl of binding buffer (10 mM HEPES pH 7.5, 1 mM EDTA and 20% dimethylformamide). After biotinylation, free biotin was washed out by purifying with RNeasy MinElute column (Qiagen, Cat#74204). 100 μl of Streptavidin C-1 bead was added to RNA and then incubated with rotating for 1 hour in binding buffer (10 mM Tris pH 7.5, 1 mM EDTA, 100 mM NaCl and 0.1% tween-20). Bead was washed 3 times with binding buffer. RNA was eluted sequentially by 5% of β-mercaptoethanol at room temperature and 100% of β-mercaptoethanol at 50°C followed by purification using RNeasy MinElute column. Purified RNA was used to qRT-PCR for quantification and normalized to relative abundance of *ACTB* RNA in 5% of input RNA which was measured by qRT-PCR. Relative abundance of nascent transcripts was calculated by ddCt method compared to non-targeting sgRNA control. Mean dCt value of each replicate was used to calculate *p*-value. Enrichment of any biotinylated-control *GAPDH* mRNA is not significantly different ($p > 0.05$). Primer sequences are listed in Table S1.

***PVT1* promoter mutagenesis—**For footprinting of regulatory element affecting cell growth (Vierstra et al., 2015), Cas9 endonuclease and sgRNA were delivered in

ribonucleotide to avoid accumulation of indels by residual nuclease activity. pET28-Cas9 plasmid was transduced into BL21-DE3 (pLysS) strain (Thermo Fisher, Cat#C6060) and Cas9 protein and sgRNA were prepared and transduced as described (Cho et al., 2014). Pre-assembled CRISPR-ribonucleoprotein complex consisting of 100 μg of Cas9 and 100 μg of sgRNA was transfected into 1×10^6 of MDA-MB-231 cells by using Amaxa Nucleofetor kit V (Lonza, Cat#VVCA-1003) with program X-013. Cells were plated on 6-well plate 3 days post-transfection (P0). Cells were passaged by 1:4 ratio every 2 days. At P10, genomic DNA was purified and 5 μg of DNA was used for PCR amplification of *PVT1* promoter region. Parallel PCR reactions were mixed and purified using AMPure beads (Beckman Coulter, #A63881) at concentrations ranging from 0.6× to 1×. Libraries were generated by nested PCR and sequenced on HiSeq 4000 with paired-end reads. Sequencing read was analyzed using CRISPresso (Pinello et al., 2016). Any variation without overlap with expected cleavage site ± 3 bp was ignored. Difference between P0 and P10 was calculated by DESeq2. To generate mutant clones, cells were diluted and plated as 0.2 cells in 96-well plate 2 days post ribonucleoprotein transfection. Genomic DNA was extracted using DNeasy 96 Blood & Tissue Kit (Qiagen, Cat#69581) and 5 to 20 μl of eluted DNA was used to PCR. Target regions were amplified from each clone and sequenced with MiSeq for genotyping. Reads from each clones were counted using Fastax-collapser. For qRT-PCR, RNA was extracted from clones at multiple passages. Primer sequences are listed in Table S1.

Targeted RNA-seq—50 ng of RNA extracted from each mNPC clone was converted to cDNA by 30 cycles of qRT-PCR reaction. Then, the region with defined SNP was amplified using 1 μl of diluted PCR product (1/20) and 15 cycles of PCR. Sequencing library was generated by 15 cycles of nested PCR using 1 μl of diluted PCR product (1/20). DNA was extracted from 1% agarose gel and sequenced on MiSeq. Reads were counted using Fastax-collapser. Reads with exactly expected sequences were considered for calculating *d*-score. The transcription level of each allele was averaged from 3 technical replicates. Primer sequences are listed in Table S1.

Allelic specific data analysis—All the sequencing data from mouse cell line were processed as described (Xu et al., 2017). The *d*-score for PVT1 expression was calculated using the first exon instead of the whole transcripts to better present the allelic different isoform of *PVT1*. The relative fold change of *MYC* was normalized to the average expression from clones with two active alleles of *PVT1*.

Deleterious score for *PVT1* promoter regions—To evaluate whether variants in the *PVT1* promoter region were potentially deleterious in the human genome, we employed the UCSC Table Browser and specified “Variation” group, “1000G ph3 Vars” track and a 5 kb window around *PVT1* transcription start sites (chr8: 128,801,802-128,811,802) to obtain VCF files for all variants. VCF files were analyzed using CADD (Kircher et al., 2014) (http://cadd.gs.washington.edu/score) to generate a C-score corresponding to the predicted deleteriousness of genome-wide variants. The CADD C-score was used to illustrate the predicted deleterious effect for each variant, which is PHRED-like (-10 × log10(rank/total)) scaled, ranking a variant relative to all possible substitutions of the human genome (8.6 ×

10^9). On this scale, variants with a C-score of greater than or equal to 10 are predicted to be amongst the top 10% most deleterious substitutions in the human genome.

Somatic mutations around *PVT1* promoter regions—Somatic mutations (SNVs) for different cancer types were obtained from the International Cancer Genome Consortium (ICGC) (Release 23). Mutations within a 5 kb window of the TSS from a set of annotated lncRNAs (ENSEMBL, release 70) were evaluated where lncRNA promoter regions from Chr 1 or Chr 8 were employed as controls. The number of somatic mutations within each lncRNA promoter region for each cancer type was used to generate a background (control) distribution against which the frequency of *PVT1* promoter mutations was evaluated.

Significance of SV overlaps in *PVT1* promoter region—Somatic structural variant (SV) calls for the ICGC BRCA-EU cohort were obtained from the original publication (Glodzik et al., 2017). The number of SVs (less than 1 million base pair in length, for duplications, deletions or inversions) overlapping with 3,826 lncRNA promoters (ENSEMBL, release 70, with gene length > 5000 bp) was calculated. Promoters were defined as [-1000, 2414] bp of the corresponding transcription start site (TSS), keeping with the definition used in this study for *PVT1*. Local background SV overlap rates were computed based on the mean overlap for windows in adjacent regions (5 million bp). Negative binomial regression was performed using the local background rate as the offset and SV overlap in each promoter as the observed variable (Nik-Zainal et al., 2016). The estimated over dispersion parameter was then used as input to a negative binomial test to evaluate the significance of SV overlap in each promoter. FDR adjusted *p*-values were employed to correct for multiple testing.

Rearrangement analysis—Fusion transcripts and their exact breakpoints were identified in RNA-seq data (Illumina, 30×) of an ER-, HER2+ breast cancer using breakpoint assembly for candidate sites with an enrichment of chimeric reads or clusters of abnormal read pairs that map to unexpectedly distant sites (Fernandez-Cuesta et al., 2015). DNA-level breakpoints associated with the fusion events were determined based on abnormal read pairs in the vicinity of the detected fusion points by analyzing whole genome sequencing (WGS) data (30×) from the same donor. The RNA-seq and WGS data for this case were generated on the Illumina platform using standard protocols. The patient (MB-0152) derives from the METABRIC cohort (Curtis et al., 2012) for which array based copy number and gene expression data were previously described.

Quantification and Statistical Analysis

In relevant figures, Figure Legends denote the statistical details of experiments including statistical tests used, kind of replicates and the value of *n*. Asterisks define degree of significance as described in the Figure Legends. All Student's *t*-test and Mann-Whitney *U*-test were analyzed in two-sided. All the sequencing data were aligned to human genome (GRCh37/hg19) or mouse genome (NCBI37/mm9) unless indicated specifically. All statistical analyses and graphics were performed using the R Statistical Programming Language and Bioconductor (Gentleman et al., 2004).

Data and Software Availability

All software used in this study is listed in KEY RESOURSES TABLE. ChromHMM was imported from Breast vHMEC from Roadmap Epigenomics Consortium. Conservation plot is imported from100 vertebrates Basewise Conservation by PhyloP at UCSC genome browser. All raw sequencing reads and raw count matrices generated in this study are available through Gene Expression Omnibus (GEO) with accession number GSE97669. Data for human cancer patient is available through European Genome-Phenome Archive (EGA) with accession number EGAD00001003342.

Supplementary Material

Refer to Web version on PubMed Central for supplementary material.

Acknowledgments

We thank members of the Chang lab for helpful discussions and assistance. We thank Seung K. Kim for access to FACS, Hokyung K. Chung for her help in microscopy imaging, and Hye Mi Jung for advice on scientific illustration. Supported by National Institutes of Health R35-CA209919, P50-HG007735 (to H.Y.C), 1R01-NS091544 (to D.A.L.), U01-CA168370, R01-DA036858 (to J.S.W.) and S10OD018220 (to Stanford Functional Genomics Facility). J.S.W. is an investigator of the Howard Hughes Medical Institute.

References

Adamson B, Norman TM, Jost M, Cho MY, Nunez JK, Chen Y, Villalta JE, Gilbert LA, Horlbeck MA, Hein MY, et al. A Multiplexed Single-Cell CRISPR Screening Platform Enables Systematic Dissection of the Unfolded ProteinResponse. Cell. 2016; 167:1867–1882 e1821. [PubMed: 27984733]

Adey A, Burton JN, Kitzman JO, Hiatt JB, Lewis AP, Martin BK, Qiu R, Lee C, Shendure J. The haplotype-resolved genome and epigenome of the aneuploid HeLa cancer cell line. Nature. 2013; 500:207–211. [PubMed: 23925245]

Anderson KM, Anderson DM, McAnally JR, Shelton JM, Bassel-Duby R, Olson EN. Transcription of the non-coding RNA upperhand controls Hand2 expression and heart development. Nature. 2016; 539:433–436. [PubMed: 27783597]

Blancafort P, Magnenat L, Barbas CF 3rd. Scanning the human genome with combinatorial transcription factor libraries. Nat Biotechnol. 2003; 21:269–274. [PubMed: 12592412]

Buenrostro JD, Wu B, Chang HY, Greenleaf WJ. ATAC-seq: A Method for Assaying Chromatin Accessibility Genome-Wide. Curr Protoc Mol Biol. 2015; 109:21 29 21–29.

Chinen Y, Sakamoto N, Nagoshi H, Taki T, Maegawa S, Tatekawa S, Tsukamoto T, Mizutani S, Shimura Y, Yamamoto-Sugitani M, et al. 8q24 amplified segments involve novel fusion genes between NSMCE2 and long noncoding RNAs in acute myelogenous leukemia. J Hematol Oncol. 2014; 7:68. [PubMed: 25245984]

Cho SW, Kim S, Kim Y, Kweon J, Kim HS, Bae S, Kim JS. Analysis of off-target effects of CRISPR/Cas-derived RNA-guided endonucleases and nickases. Genome Res. 2014; 24:132–141. [PubMed: 24253446]

Claveria C, Giovinazzo G, Sierra R, Torres M. Myc-driven endogenous cell competition in the early mammalian embryo. Nature. 2013; 500:39–44. [PubMed: 23842495]

Cleary MD, Meiering CD, Jan E, Guymon R, Boothroyd JC. Biosynthetic labeling of RNA with uracil phosphoribosyltransferase allows cell-specific microarray analysis of mRNA synthesis and decay. Nat Biotechnol. 2005; 23:232–237. [PubMed: 15685165]

Csorba T, Questa JI, Sun Q, Dean C. Antisense COOLAIR mediates the coordinated switching of chromatin states at FLC during vernalization. Proc Natl Acad Sci U S A. 2014; 111:16160–16165. [PubMed: 25349421]

Curtis C, Shah SP, Chin SF, Turashvili G, Rueda OM, Dunning MJ, Speed D, Lynch AG, Samarajiwa S, Yuan Y, et al. The genomic and transcriptomic architecture of 2,000 breast tumours reveals novel subgroups. Nature. 2012; 486:346–352. [PubMed: 22522925]

Derrien T, Johnson R, Bussotti G, Tanzer A, Djebali S, Tilgner H, Guernec G, Martin D, Merkel A, Knowles DG, et al. The GENCODE v7 catalog of human long noncoding RNAs: analysis of their gene structure, evolution, and expression. Genome Res. 2012; 22:1775–1789. [PubMed: 22955988]

Devaiah BN, Lewis BA, Cherman N, Hewitt MC, Albrecht BK, Robey PG, Ozato K, Sims RJ 3rd, Singer DS. BRD4 is an atypical kinase that phosphorylates serine2 of the RNA polymerase II carboxy-terminal domain. Proc Natl Acad Sci U S A. 2012; 109:6927–6932. [PubMed: 22509028]

Dixon JR, Selvaraj S, Yue F, Kim A, Li Y, Shen Y, Hu M, Liu JS, Ren B. Topological domains in mammalian genomes identified by analysis of chromatin interactions. Nature. 2012; 485:376–380. [PubMed: 22495300]

Duffy EE, Rutenberg-Schoenberg M, Stark CD, Kitchen RR, Gerstein MB, Simon MD. Tracking Distinct RNA Populations Using Efficient and Reversible Covalent Chemistry. Mol Cell. 2015; 59:858–866. [PubMed: 26340425]

Engreitz JM, Haines JE, Perez EM, Munson G, Chen J, Kane M, McDonel PE, Guttman M, Lander ES. Local regulation of gene expression by lncRNA promoters, transcription and splicing. Nature. 2016; 539:452–455. [PubMed: 27783602]

Fatica A, Bozzoni I. Long non-coding RNAs: new players in cell differentiation and development. Nat Rev Genet. 2014; 15:7–21. [PubMed: 24296535]

Fernandez-Cuesta L, Sun R, Menon R, George J, Lorenz S, Meza-Zepeda LA, Peifer M, Plenker D, Heuckmann JM, Leenders F, et al. Identification of novel fusion genes in lung cancer using breakpoint assembly of transcriptome sequencing data. Genome Biol. 2015; 16:7. [PubMed: 25650807]

Filippakopoulos P, Qi J, Picaud S, Shen Y, Smith WB, Fedorov O, Morse EM, Keates T, Hickman TT, Felletar I, et al. Selective inhibition of BET bromodomains. Nature. 2010; 468:1067–1073. [PubMed: 20871596]

Flavahan WA, Drier Y, Liau BB, Gillespie SM, Venteicher AS, Stemmer-Rachamimov AO, Suva ML, Bernstein BE. Insulator dysfunction and oncogene activation in IDH mutant gliomas. Nature. 2016; 529:110–114. [PubMed: 26700815]

Fulco CP, Munschauer M, Anyoha R, Munson G, Grossman SR, Perez EM, Kane M, Cleary B, Lander ES, Engreitz JM. Systematic mapping of functional enhancer-promoter connections with CRISPR interference. Science. 2016; 354:769–773. [PubMed: 27708057]

Gentleman RC, Carey VJ, Bates DM, Bolstad B, Dettling M, Dudoit S, Ellis B, Gautier L, Ge Y, Gentry J, et al. Bioconductor: open software development for computational biology and bioinformatics. Genome Biol. 2004; 5:R80. [PubMed: 15461798]

Gilbert LA, Horlbeck MA, Adamson B, Villalta JE, Chen Y, Whitehead EH, Guimaraes C, Panning B, Ploegh HL, Bassik MC, et al. Genome-Scale CRISPR-Mediated Control of Gene Repression and Activation. Cell. 2014; 159:647–661. [PubMed: 25307932]

Gilbert LA, Larson MH, Morsut L, Liu Z, Brar GA, Torres SE, Stern-Ginossar N, Brandman O, Whitehead EH, Doudna JA, et al. CRISPR-mediated modular RNA-guided regulation of transcription in eukaryotes. Cell. 2013; 154:442–451. [PubMed: 23849981]

Glodzik D, Morganella S, Davies H, Simpson PT, Li Y, Zou X, Diez-Perez J, Staaf J, Alexandrov LB, Smid M, et al. A somatic-mutational process recurrently duplicates germline susceptibility loci and tissue-specific super-enhancers in breast cancers. Nat Genet. 2017; 49:341–348. [PubMed: 28112740]

Graham M, Adams JM. Chromosome 8 breakpoint far 3′ of the c-myc oncogene in a Burkitt's lymphoma 2;8 variant translocation is equivalent to the murine pvt-1 locus. EMBO J. 1986; 5:2845–2851. [PubMed: 3024964]

Groff AF, Sanchez-Gomez DB, Soruco MML, Gerhardinger C, Barutcu AR, Li E, Elcavage L, Plana O, Sanchez LV, Lee JC, et al. In Vivo Characterization of Linc-p21 Reveals Functional cis-Regulatory DNA Elements. Cell Rep. 2016; 16:2178–2186. [PubMed: 27524623]

Hon CC, Ramilowski JA, Harshbarger J, Bertin N, Rackham OJ, Gough J, Denisenko E, Schmeier S, Poulsen TM, Severin J, et al. An atlas of human long non-coding RNAs with accurate 5′ ends. Nature. 2017; 543:199–204. [PubMed: 28241135]

Kenny PA, Lee GY, Myers CA, Neve RM, Semeiks JR, Spellman PT, Lorenz K, Lee EH, Barcellos-Hoff MH, Petersen OW, et al. The morphologies of breast cancer cell lines in three-dimensional assays correlate with their profiles of gene expression. Mol Oncol. 2007; 1:84–96. [PubMed: 18516279]

Kim D, Langmead B, Salzberg SL. HISAT: a fast spliced aligner with low memory requirements. Nat Methods. 2015; 12:357–360. [PubMed: 25751142]

Kim D, Pertea G, Trapnell C, Pimentel H, Kelley R, Salzberg SL. TopHat2: accurate alignment of transcriptomes in the presence of insertions, deletions and gene fusions. Genome Biol. 2013; 14:R36. [PubMed: 23618408]

Kim HP, Cho GA, Han SW, Shin JY, Jeong EG, Song SH, Lee WC, Lee KH, Bang D, Seo JS, et al. Novel fusion transcripts in human gastric cancer revealed by transcriptome analysis. Oncogene. 2014a; 33:5434–5441. [PubMed: 24240688]

Kircher M, Witten DM, Jain P, O'Roak BJ, Cooper GM, Shendure J. A general framework for estimating the relative pathogenicity of human genetic variants. Nat Genet. 2014; 46:310–315. [PubMed: 24487276]

Konermann S, Brigham MD, Trevino AE, Joung J, Abudayyeh OO, Barcena C, Hsu PD, Habib N, Gootenberg JS, Nishimasu H, et al. Genome-scale transcriptional activation by an engineered CRISPR-Cas9 complex. Nature. 2015; 517:583–588. [PubMed: 25494202]

Kress TR, Sabo A, Amati B. MYC: connecting selective transcriptional control to global RNA production. Nat Rev Cancer. 2015; 15:593–607. [PubMed: 26383138]

Langmead B, Salzberg SL. Fast gapped-read alignment with Bowtie 2. Nat Methods. 2012; 9:357–359. [PubMed: 22388286]

Li H, Handsaker B, Wysoker A, Fennell T, Ruan J, Homer N, Marth G, Abecasis G, Durbin R. Genome Project Data Processing S. The Sequence Alignment/Map format and SAMtools. Bioinformatics. 2009; 25:2078–2079. [PubMed: 19505943]

Liu SJ, Horlbeck MA, Cho SW, Birk HS, Malatesta M, He D, Attenello FJ, Villalta JE, Cho MY, Chen Y, et al. CRISPRi-based genome-scale identification of functional long noncoding RNA loci in human cells. Science. 2017; 355

Love MI, Huber W, Anders S. Moderated estimation of fold change and dispersion for RNA-seq data with DESeq2. Genome Biol. 2014; 15:550. [PubMed: 25516281]

Lupianez DG, Kraft K, Heinrich V, Krawitz P, Brancati F, Klopocki E, Horn D, Kayserili H, Opitz JM, Laxova R, et al. Disruptions of topological chromatin domains cause pathogenic rewiring of gene-enhancer interactions. Cell. 2015; 161:1012–1025. [PubMed: 25959774]

Miller BE, Miller FR, Wilburn D, Heppner GH. Dominance of a tumor subpopulation line in mixed heterogeneous mouse mammary tumors. Cancer Res. 1988; 48:5747–5753. [PubMed: 3167832]

Mumbach MR, Rubin AJ, Flynn RA, Dai C, Khavari PA, Greenleaf WJ, Chang HY. HiChIP: efficient and sensitive analysis of protein-directed genome architecture. Nat Methods. 2016; 13:919–922. [PubMed: 27643841]

Mumbach MR, Satpathy AT, Boyle EA, Dai C, Gowen BG, Cho SW, Nguyen ML, Rubin AJ, Granja JM, Kazane KR, et al. Enhancer connectome in primary human cells identifies target genes of disease-associated DNA elements. Nat Genet. 2017

Nagoshi H, Taki T, Hanamura I, Nitta M, Otsuki T, Nishida K, Okuda K, Sakamoto N, Kobayashi S, Yamamoto-Sugitani M, et al. Frequent PVT1 rearrangement and novel chimeric genes PVT1-NBEA and PVT1-WWOX occur in multiple myeloma with 8q24 abnormality. Cancer Res. 2012; 72:4954–4962. [PubMed: 22869583]

Nik-Zainal S, Davies H, Staaf J, Ramakrishna M, Glodzik D, Zou X, Martincorena I, Alexandrov LB, Martin S, Wedge DC, et al. Landscape of somatic mutations in 560 breast cancer whole-genome sequences. Nature. 2016; 534:47–54. [PubMed: 27135926]

Northcott PA, Shih DJ, Peacock J, Garzia L, Morrissy AS, Zichner T, Stutz AM, Korshunov A, Reimand J, Schumacher SE, et al. Subgroup-specific structural variation across 1,000 medulloblastoma genomes. Nature. 2012; 488:49–56. [PubMed: 22832581]

Park KS, Lee DK, Lee H, Lee Y, Jang YS, Kim YH, Yang HY, Lee SI, Seol W, Kim JS. Phenotypic alteration of eukaryotic cells using randomized libraries of artificial transcription factors. Nat Biotechnol. 2003; 21:1208–1214. [PubMed: 12960965]

Pinello L, Canver MC, Hoban MD, Orkin SH, Kohn DB, Bauer DE, Yuan GC. Analyzing CRISPR genome-editing experiments with CRISPResso. Nat Biotechnol. 2016; 34:695–697. [PubMed: 27404874]

Pleasance ED, Stephens PJ, O'Meara S, McBride DJ, Meynert A, Jones D, Lin ML, Beare D, Lau KW, Greenman C, et al. A small-cell lung cancer genome with complex signatures of tobacco exposure. Nature. 2010; 463:184–190. [PubMed: 20016488]

Pombo A, Dillon N. Three-dimensional genome architecture: players and mechanisms. Nat Rev Mol Cell Biol. 2015; 16:245–257. [PubMed: 25757416]

Quinlan AR, Hall IM. BEDTools: a flexible suite of utilities for comparing genomic features. Bioinformatics. 2010; 26:841–842. [PubMed: 20110278]

Ram O, Goren A, Amit I, Shoresh N, Yosef N, Ernst J, Kellis M, Gymrek M, Issner R, Coyne M, et al. Combinatorial patterning of chromatin regulators uncovered by genome-wide location analysis in human cells. Cell. 2011; 147:1628–1639. [PubMed: 22196736]

Schmitt AM, Chang HY. Long Noncoding RNAs in Cancer Pathways. Cancer Cell. 2016; 29:452–463. [PubMed: 27070700]

Schwartzman O, Mukamel Z, Oded-Elkayam N, Olivares-Chauvet P, Lubling Y, Landan G, Izraeli S, Tanay A. UMI-4C for quantitative and targeted chromosomal contact profiling. Nat Methods. 2016; 13:685–691. [PubMed: 27376768]

Scruggs BS, Adelman K. The Importance of Controlling Transcription Elongation at Coding and Noncoding RNA Loci. Cold Spring Harb Symp Quant Biol. 2015; 80:33–44. [PubMed: 27325707]

Servant N, Varoquaux N, Lajoie BR, Viara E, Chen CJ, Vert JP, Heard E, Dekker J, Barillot E. HiC-Pro: an optimized and flexible pipeline for Hi-C data processing. Genome Biol. 2015; 16:259. [PubMed: 26619908]

Shtivelman E, Bishop JM. Effects of translocations on transcription from PVT. Mol Cell Biol. 1990; 10:1835–1839. [PubMed: 2181290]

Shtivelman E, Henglein B, Groitl P, Lipp M, Bishop JM. Identification of a human transcription unit affected by the variant chromosomal translocations 2;8 and 8;22 of Burkitt lymphoma. Proc Natl Acad Sci U S A. 1989; 86:3257–3260. [PubMed: 2470097]

Sotelo J, Esposito D, Duhagon MA, Banfield K, Mehalko J, Liao H, Stephens RM, Harris TJ, Munroe DJ, Wu X. Long-range enhancers on 8q24 regulate c-Myc. Proc Natl Acad Sci U S A. 2010; 107:3001–3005. [PubMed: 20133699]

Stadhouders R, Kolovos P, Brouwer R, Zuin J, van den Heuvel A, Kockx C, Palstra RJ, Wendt KS, Grosveld F, van Ijcken W, et al. Multiplexed chromosome conformation capture sequencing for rapid genome-scale high-resolution detection of long-range chromatin interactions. Nat Protoc. 2013; 8:509–524. [PubMed: 23411633]

Sur IK, Hallikas O, Vaharautio A, Yan J, Turunen M, Enge M, Taipale M, Karhu A, Aaltonen LA, Taipale J. Mice lacking a Myc enhancer that includes human SNP rs6983267 are resistant to intestinal tumors. Science. 2012; 338:1360–1363. [PubMed: 23118011]

Tseng YY, Moriarity BS, Gong W, Akiyama R, Tiwari A, Kawakami H, Ronning P, Reuland B, Guenther K, Beadnell TC, et al. PVT1 dependence in cancer with MYC copy-number increase. Nature. 2014; 512:82–86. [PubMed: 25043044]

Vierstra J, Reik A, Chang KH, Stehling-Sun S, Zhou Y, Hinkley SJ, Paschon DE, Zhang L, Psatha N, Bendana YR, et al. Functional footprinting of regulatory DNA. Nat Methods. 2015; 12:927–930. [PubMed: 26322838]

Wang F, Yuan JH, Wang SB, Yang F, Yuan SX, Ye C, Yang N, Zhou WP, Li WL, Li W, et al. Oncofetal long noncoding RNA PVT1 promotes proliferation and stem cell-like property of hepatocellular carcinoma cells by stabilizing NOP2. Hepatology. 2014a; 60:1278–1290. [PubMed: 25043274]

Xiang JF, Yin QF, Chen T, Zhang Y, Zhang XO, Wu Z, Zhang S, Wang HB, Ge J, Lu X, et al. Human colorectal cancer-specific CCAT1-L lncRNA regulates long-range chromatin interactions at the MYC locus. Cell Res. 2014; 24:513–531. [PubMed: 24662484]

Xu J, Carter AC, Gendrel AV, Attia M, Loftus J, Greenleaf WJ, Tibshirani R, Heard E, Chang HY. Landscape of monoallelic DNA accessibility in mouse embryonic stem cells and neural progenitor cells. Nat Genet. 2017a; 49:377–386. [PubMed: 28112738]

Xu MD, Wang Y, Weng W, Wei P, Qi P, Zhang Q, Tan C, Ni SJ, Dong L, Yang Y, et al. A Positive Feedback Loop of lncRNA-PVT1 and FOXM1 Facilitates Gastric Cancer Growth and Invasion. Clin Cancer Res. 2017b; 23:2071–2080. [PubMed: 27756785]

Yin Y, Yan P, Lu J, Song G, Zhu Y, Li Z, Zhao Y, Shen B, Huang X, Zhu H, et al. Opposing Roles for the lncRNA Haunt and Its Genomic Locus in Regulating HOXA Gene Activation during Embryonic Stem Cell Differentiation. Cell Stem Cell. 2015; 16:504–516. [PubMed: 25891907]

Zhang X, Choi PS, Francis JM, Imielinski M, Watanabe H, Cherniack AD, Meyerson M. Identification of focally amplified lineage-specific super-enhancers in human epithelial cancers. Nat Genet. 2016; 48:176–182. [PubMed: 26656844]

Zhang Y, Liu T, Meyer CA, Eeckhoute J, Johnson DS, Bernstein BE, Nusbaum C, Myers RM, Brown M, Li W, et al. Model-based analysis of ChIP-Seq (MACS). Genome Biol. 2008; 9:R137. [PubMed: 18798982]

Highlights

- Silencing *PVT1* promoter enhances breast cancer cell competition.
- *PVT1* promoter inhibits *MYC* transcription independent of PVT1 lncRNA.
- *PVT1* and *MYC* promoters compete for enhancer contact in *cis*.
- Mutations encompassing *PVT1* promoter are recurrent in human cancers

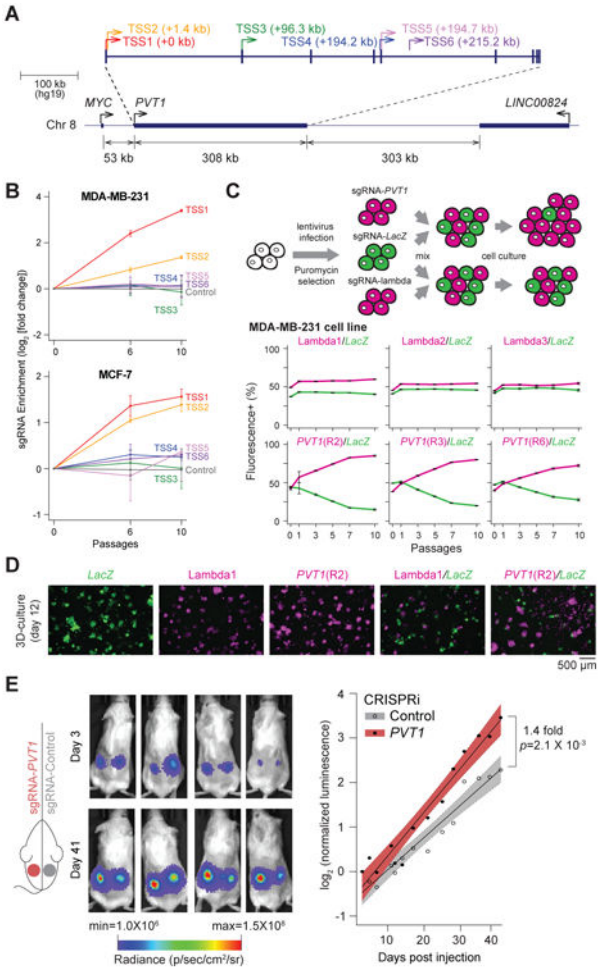

Figure 1. CRISPRi-*PVT1* enhanced cancer cell proliferation

A, Schematic representing the *PVT1* locus and six TSS of *PVT1*. **B**, Enrichment of sgRNAs targeting *PVT1* in two breast cancer cell lines at indicated passages. Error bars indicate mean ± SD for top 3 sgRNAs targeting each TSS. **C**, Cell growth competition assay for CRISPRi-*PVT1* in MDA-MB-231 cell line. Schematic representation of the assay (upper). Plots showing percentage of mCherry+ or GFP+ cells at indicated passages (bottom). Error bars indicate mean ± SD (n=3, technical replicates). **D**, Fluorescence microscopy image of cell growth competition assay by 3D cell culture of MDA-MB-231 cell line. For **C** and **D**, target genes of sgRNA are shown in the same color as of the fluorescent marker above each panel. **E**, Tumor growth of subcutaneous xenografted MDA-MB-231 with CRISPRi-Control or CRISPRi-*PVT1* (R2). Luminescence images at day 3 or day 41 post injection(left). Fitted growth curve of injected tumor cells (right). p-value was calculated by paired Mann-Whitney U-test (n=12 for each). Shaded region indicates 95% confidence intervals.

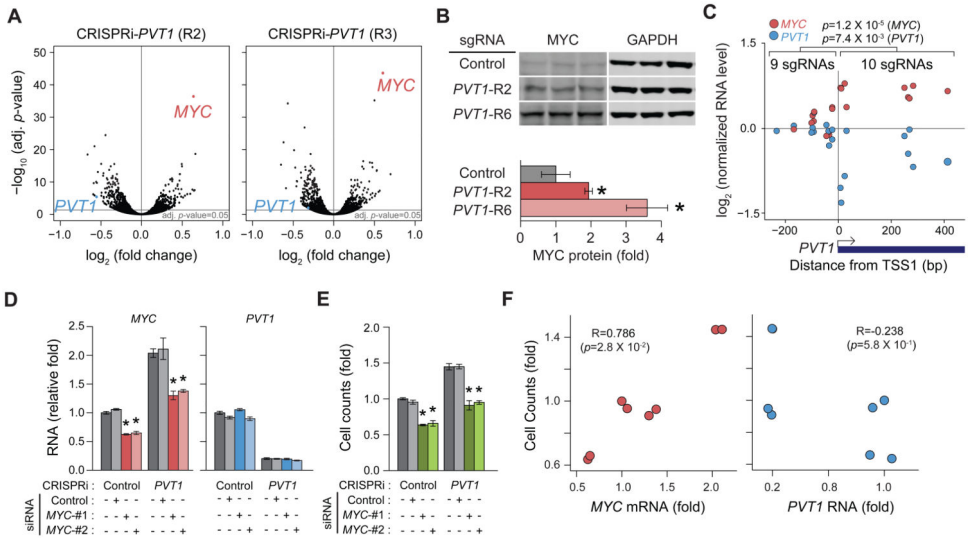

Figure 2. Pro-growth phenotype was induced by increased *MYC* expression in MDA-MB-231 cell line

A, RNA-seq results comparing CRISPRi-Control and CRISPRi-*PVT1* cell line (n=2, biological replicates). **B**, Western blot analysis for MYC protein changed by CRISPRi-*PVT1* (top) and relative quantification of MYC protein (bottom). Error bars indicate mean ± SD. (n=3, biological replicates). **C**, Comparison of *MYC* and *PVT1* RNA level between CRISPRi targeting upstream and downstream of *PVT1*-TSS1. p-values were calculated by unpaired Mann-Whitney U-test. **D** and **E**, qRT-PCR for relative RNA levels of *MYC* and *PVT1* (**D**) or relative cell counts at day 4 post transfection (**E**) with siRNA targeting *MYC* with CRISPRi-Control or CRISPRi-*PVT1* (R2). Error bars indicate mean ± SEM (n=3, biological replicates). **F**, Correlation between relative cell counts and *MYC* (left) or *PVT1* (right) RNA level described in Figure 2D and 2E. Spearman's coefficient (R) and p-value are shown. *p<0.05, using unpaired t-test compared with control (dark grey).

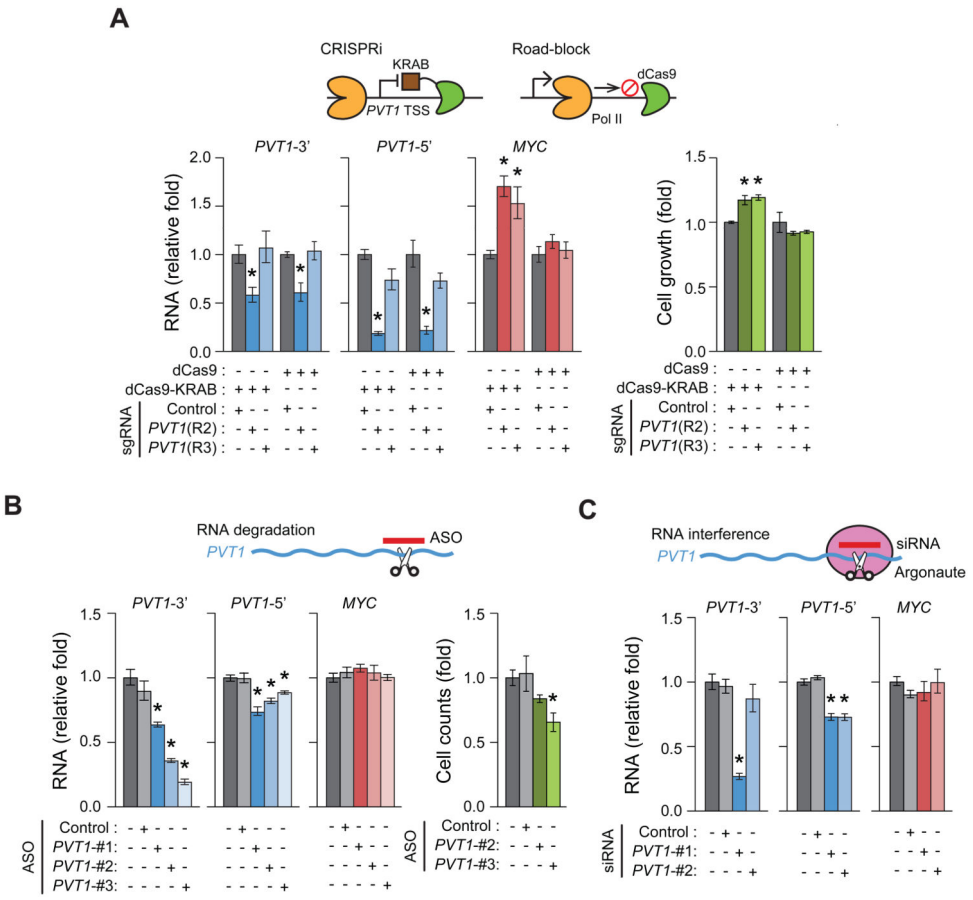

Figure 3. *PVT1* lncRNA independent mechanism for *MYC* induction in MDA-MB-231 cell line

A, qRT-PCR for relative RNA level of *MYC* or *PVT1* (left) or relative cell growth at day 4 post plating (right) for sgRNA-Control or sgRNA-*PVT1* with dCas9-KRAB or dCas9. Relative cell growth was measured by MTT assay. **B**, qRT-PCR for relative RNA levels of *MYC* and *PVT1* (left) or relative cell count at day 4 post transfection (right) with ASO targeting *PVT1*. **C**, qRT-PCR for relative RNA levels of *MYC* and *PVT1* with siRNA targeting *PVT1*. Schematic representation for each experiment is shown above each plot. Error bars indicate mean ± SEM (n=3, biological replicates). *p<0.05, using unpaired t-test compared with control (dark grey).

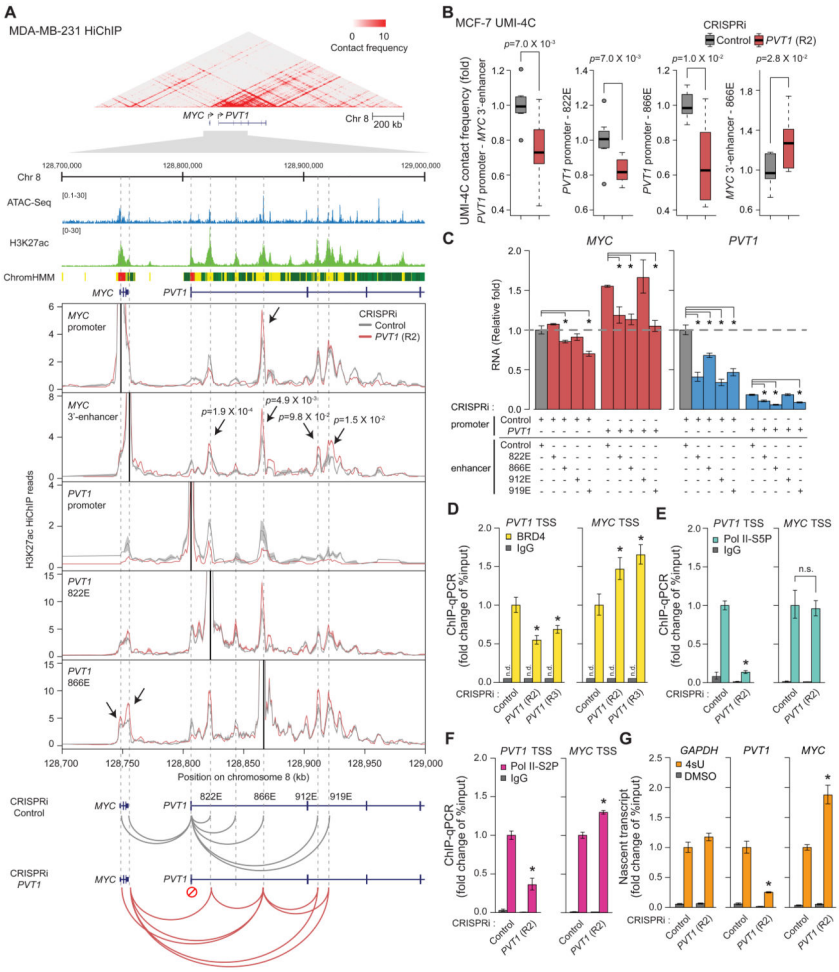

Figure 4. *PVT1* promoter suppresses *MYC* transcription by competing for *PVT1* intragenic enhancers

A, *PVT1* promoter functions as a boundary element in MDA-MB-231 cell line. Top: Heat-map representing chromatin conformation around *PVT1* locus measured by H3K27ac HiChIP (n=2, biological replicates). ATAC-seq peaks, H3K27ac ChIP-seq peaks and ChromHMM diagram are shown to indicate enhancer elements. Middle: Virtual 4C plots showing H3K27ac HiChIP contact frequency at 1 kb resolution anchored at each indicated genomic position (solid black lines) with CRISPRi-Control or CRISPRi-*PVT1*. Bottom: Schematic diagram showing changes in chromosome interaction induced by CRISRPi-*PVT1*. Shaded region indicates mean ± SEM (n=2, biological replicates). p-value of each interaction between *MYC* 3′-enhancer and *PVT1* intragenic enhancer was calculated by Fisher's exact test. **B**, Boxplots showing chromosome contact frequency at 5 kb resolution measured by UMI-4C in MCF-7 cell line with CRISPRi-Control or CRISPRi-*PVT1* (R2). p-value was calculated by un-paired Mann-Whitney U-test (n=8). **C,** qRT-PCR for relative RNA level of *MYC* and *PVT1* with dual CRISPRi targeting *PVT1* promoter or intragenic enhancers in MDA-MB-231 cell line. The difference between single CRISPRi-*PVT1* and dual CRISPRi-*PVT1* with CRISPRi-enhancer (822E, 866E or 919E) is not significant (p>0.05). **D** to **F**, ChIP-qPCR representing relative *PVT1* or *MYC* promoter DNA bound to BRD4 (**D**), Pol II-S5P (**E**), Pol II-S2P (**F**) in MDA-MB-231 cell line with CRISPRi-control

or CRISPRi-*PVT1*. **G**, qRT-PCR for the relative level of 4sU-labeled nascent transcripts of *PVT1* or *MYC* in MDA-MB-231 cell line with CRISPRi-control or CRISPRi-*PVT1*. Error bars indicate mean ± SEM (n=3, biological replicates). *p<0.05, using unpaired t-test compared with control (dark grey). n.s., not significant (p>0.05); n.d., not detected. See also **STAR METHOD** for details.

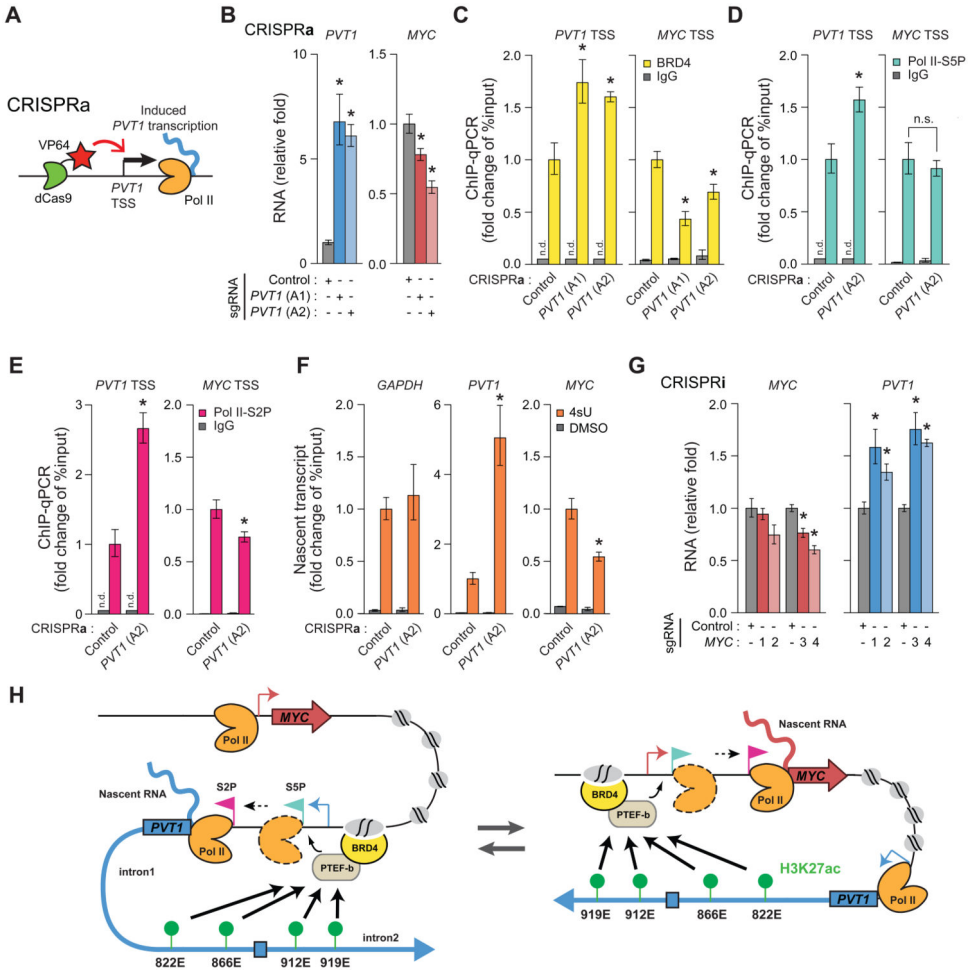

Figure 5. *PVT1* reversibly regulates *MYC* transcription in MDA-MB-231 cell line

A, Schematic representing CRISPRa at *PVT1* promoter. **B**, qRT-PCR for *PVT1* or *MYC* with CRISPRa-control or CRISPRa-*PVT1*. **C** to **E**, ChIP-qPCR for *PVT1* or *MYC* TSS for BRD4 (**C**), Pol II-S5P (**D**) or Pol II-S2P (**E**) with CRISPRa-Control or CRISPRa-*PVT1*. **F**, qRT-PCR for relative level of 4sU-labeled nascent transcripts with CRISPRa-Control or CRISPRa-*PVT1*. **G**, qRT-PCR for *PVT1* or *MYC* with CRISPRi-Control or CRISPRi-*MYC*. **H**, Schematic representing the model of promoter-enhancer competition between *PVT1* and *MYC*. Error bars indicate mean ± SEM (n=3, biological replicates). *p<0.05, using un-paired t-test compared with control (grey). n.s., not significant (p>0.05); n.d., not detected.

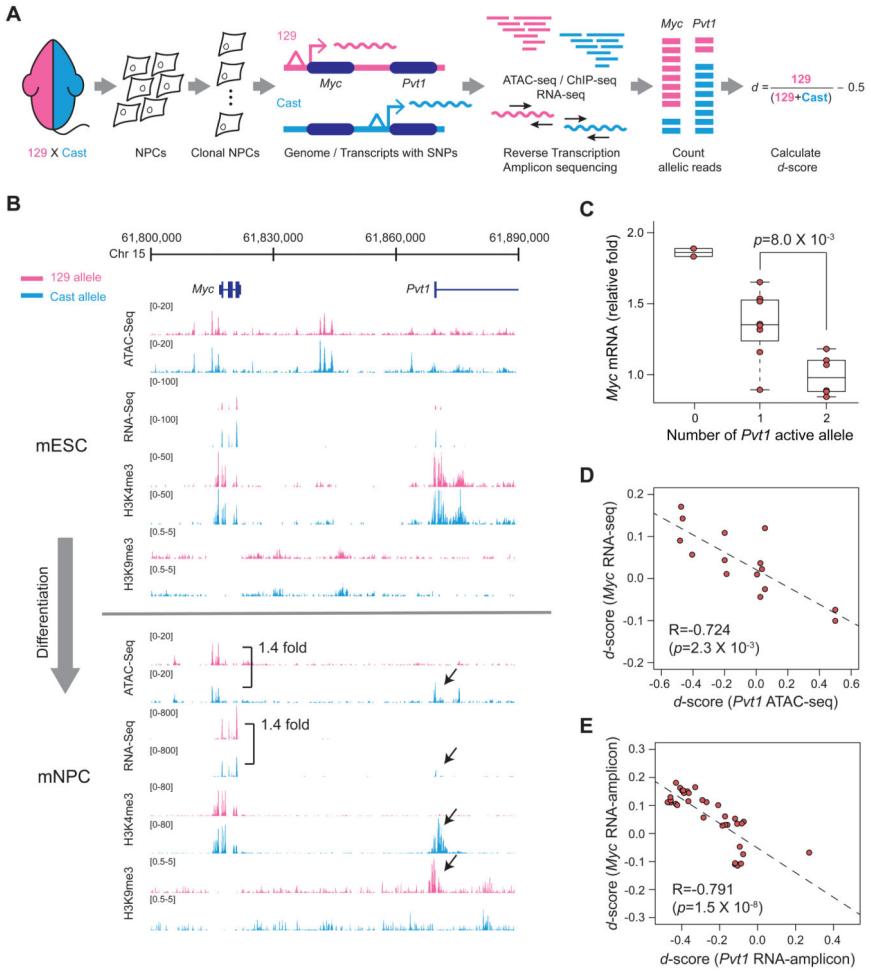

Figure 6. *PVT1* promoter regulates *MYC* expression *in cis* and allele-specific manner

A, Schematic representing experiments for allele-specific regulation**. B**, ATAC-seq, RNA-seq, H3K9me3 or H3K4me3 signals around *PVT1-MYC* locus measured in mESC or mNPC derived from a hybrid mouse. Reads with SNPs corresponding to the 129 or Cast allele are shown as pink or blue, respectively. **C**, Box plot showing *MYC* mRNA level according to the number of active *PVT1* alleles. *p*-value was calculated by unpaired Mann-Whitney *U*-test. **D,** Correlation between the *d*-score for accessibility of the *PVT1* locus from ATAC-seq and *MYC* transcription level from RNA-seq. For **C** and **D**, *n*=15 from 11 clones and 4 additional technical replicates. **E,** Correlation between *d*-score of RNA level measured by targeted RNA-seq (*n*=35). For **D** and **E**, Spearman's coefficient (R) and *p*-value are shown.

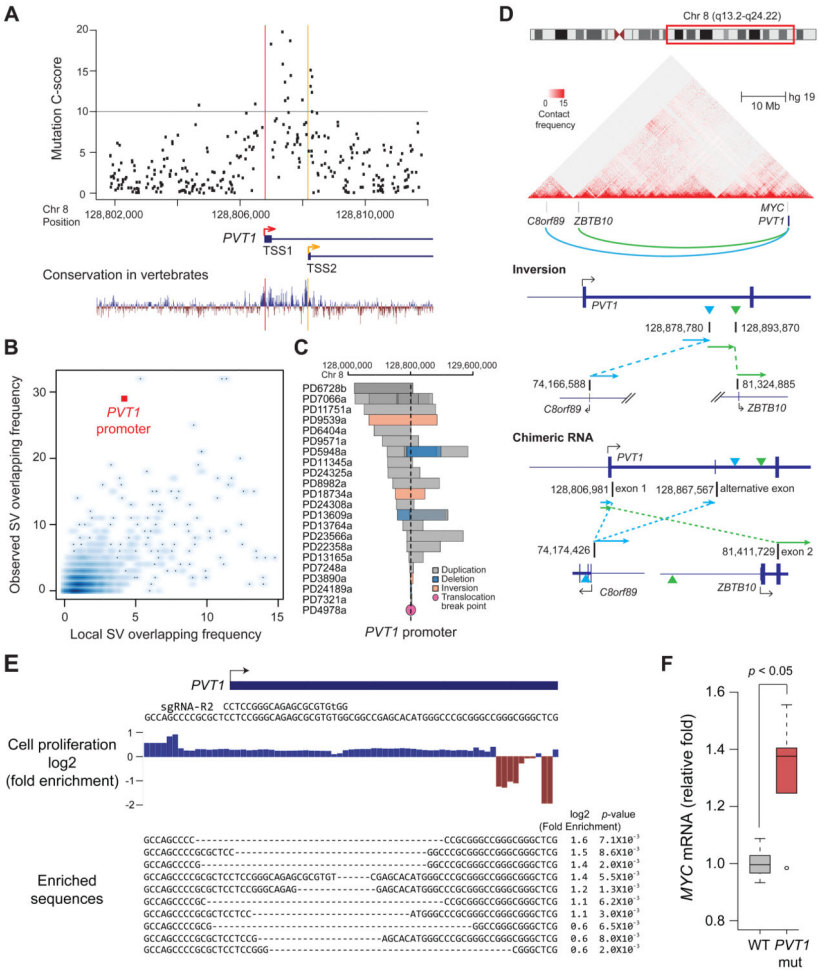

Figure 7. *PVT1* promoter functions as a tumor suppressor

A, Scatter plot representing C-scores for variants at *PVT1*-TSS ± 5 kb region from CADD analysis (upper) and conservation plot (bottom). Grey line indicates C-score=10, top 10%. TSS1 or TSS2 of *PVT1* is shown as a red or yellow line, respectively. **B**, Number of SVs including duplications, deletions and inversions overlapping with lncRNA promoter in the BRCA-EU cohort (y-axis). Basal SV frequency was measured in adjacent windows within 5 megabase (x-axis). See also STAR METHOD. **C**, SVs encompassing the *PVT1* promoter in breast tumor patients. The patient ID is shown on the left. **D**, Genomic structure showing a recurrent intra-chromosomal inversion within *PVT1* intron 1 in breast tumor patients. Ideogram of Chr. 8, heat-map of chromatin conformation within indicated region (top), inversion in genomic context (middle) and fusion transcription found in this tumor (bottom) were shown. **E**, Footprinting for regulatory element of *PVT1* promoter. Fold changes of each base or alleles after 10 passages (for $p<0.01$) were listed. **F**, Relative *MYC* mRNA level compared between MDA-MB-231 cells harboring unmodified or mutant allele of *PVT1* promoter. p-value was calculated by using unpaired Mann-Whitney U-test ($n=6$ for each).

Key Resources Table

Reagent or resource	Source	Identifier
Antibodies		
Rabbit polyclonal anti-H3 acetyl-K27	Abcam	Cat#ab4729; RRID: AB_2118291
Rabbit polyclonal anti-H3 trimethyl-K9	Abcam	Cat#ab8898; RRID: AB_306848
Rabbit polyclonal anti-H3 trimethyl-K4	Active Motif	Cat#39159; RRID: AB_2615077
Rabbit polyclonal anti-BRD4	Bethyl Laboratories	Cat#A301-985A; RRID: AB_1576498
Mouse monoclonal anti-HA	Cell Signaling	Cat#2367; RRID: AB_10691311
Rabbit polyclonal anti-Pol II phospho-Ser2	Abcam	Cat#ab5095; RRID: AB_304749
Rabbit polyclonal anti-Pol II phospho-Ser5	Abcam	Cat#ab5131; RRID: AB_449369
Rabbit polyclonal IgG	Abcam	Cat#ab171870; RRID: AB_2687657
Mouse polyclonal IgG	EMD Millipore	Cat#12-371; RRID: AB_145840
Mouse monoclonal anti-GAPDH (7B)	Santa Cruz	Cat#sc69778; RRID: AB_1124759
Rabbit monoclonal anti-MYC (D84C12)	Cell Signaling	Cat#5605S; RRID: AB_1903938
IRDye 800CW Goat anti-mouse IgG	LI-CORBioScience	Cat#926-32211; RRID: AB_621843
IRdye 680RD Goat anti-rabbitIgG	LI-CORBioScience	Cat#926-68070; RRID: AB_10956588
Bacterial and Virus Strains		
One Shot Stbl3 Chemically Competent *E.coli*	Thermo Fisher	Cat#C737303
NEB Turbo Competent *E.coli*	NEB	Cat#C2984H
One Shot BL21(DE3) pLysS Chemically Competent *E. coli*	Thermo Fisher	Cat#C606003
Chemicals, Peptides, and Recombinant Proteins		
Proteinase K, Molecular Biology Grade	NEB	Cat#P8107S
Quick Ligation Kit	NEB	Cat#M2200L
Klenow Fragment (3′-5′exo-)	NEB	Cat#M0212L
NEBNext End Repair Module	NEB	Cat#E6050L
Adenosine 5′-Triphosphate	NEB	Cat#P0756S
T4 DNA Ligase	NEB	Cat#M0202L
MboI restriction enzyme	NEB	Cat#R0147M
Alkaline Phosphatase, Calf Intestinal	NEB	Cat#M0290L
Hot Start Taq DNA Polymerase	NEB	Cat#M0495L
NEBNext® High-Fidelity 2X PCR Master Mix	NEB	Cat#M0541L
Deoxynucleotide (dNTP) Solution Set	NEB	Cat#N0446S
NEBuilder® HiFi DNA Assembly Master Mix	NEB	Cat#E2621L
Recombinant Human FGF-basic	PeproTech	Cat#100-18B
Epidermal Growth Factor	PeproTech	Cat#315-09
MEGAshortscript T7 Transcription kit	Thermo Fisher	Cat#AM1354
MEGAclearTransription Clean-Up kit	Thermo Fisher	Cat#AM1908
Lipofectamine 3000 transfection Reagent	Thermo Fisher	Cat#L3000-015
Lipofectamine 2000 transfection Reagent	Thermo Fisher	Cat#11668-019

Reagent or resource	Source	Identifier
Hygromycin B	Thermo Fisher	Cat#10687010
Puromycin dihydrochloride	Thermo Fisher	Cat#A11138-03
Blasticidin S HCl	Thermo Fisher	Cat#A1113903
Neurobasal Medium	Thermo Fisher	Cat#21103-049
DMEM/f12	Thermo Fisher	Cat#11320-082
B-27 Supplemnet (50X), serum free	Thermo Fisher	Cat#17504044
EGF Recombinant Human Protein	Thermo Fisher	Cat#PHG0311
DynabeadsMyOne Streptavidin C1	Thermo Fisher	Cat#65002
DynabeadsProtein A for Immunoprecipitation	Thermo Fisher	Cat#10002D
Dynabeads Protein G for Immunoprecipitation	Thermo Fisher	Cat#10004D
16% Formaldehyde (w/v), Methanol-free	Thermo Fisher	Cat#28908
TrypLE Express Enzyme (1X)	Thermo Fisher	Cat#12604039
Pierce Detergent Compatible Bradford Assay Kit	Thermo Fisher	Cat#23246
SuperScript III Reverse Transcriptase	Thermo Fisher	Cat#18080-044
DMEM	Thermo Fisher	Cat#11995
Penicillin-Streptomycin	Thermo Fisher	Cat#15140163
McCoy's 5A	Thermo Fisher	Cat#16600
Horse serum	Thermo Fisher	Cat#16050122
Click-IT Biotin DIBO Alkyne	Thermo Fisher	Cat#C10412
NorthernMax™ Formaldehyde Load Dye	Thermo Fisher	Cat#AM8550
BrightStar™-Plus Positively Charged Nylon Membrane	Thermo Fisher	Cat#AM10104
NorthernMax™ One-Hour Transfer Buffer	Thermo Fisher	Cat#AM8672
ULTRAhyb™-Oligo Buffer	Thermo Fisher	Cat#AM8663
NorthernMax™ Low Stringency Wash Buffer	Thermo Fisher	Cat#AM8673
NorthernMax™ High Stringency Wash Buffer	Thermo Fisher	Cat#AM8674
Insulin from bovine pancreas	Sigma Aldrich	Cat#I1882
Cholera Toxin from Vibrio cholerae	Sigma Aldrich	Cat#C8052
4-Thiouridine	Sigma Aldrich	Cat#T4509
(+)-JQ1	Sigma Aldrich	Cat#SML1524
Hydrocortisone	Sigma Aldrich	Cat#H0888
Hexadimethrine bromide	Sigma Aldrich	Cat#107689
Odyssey Blocking Buffer (PBS)	LI-COR BioScience	Cat#927-40003
Streptavidin-IRDye 800CW	LI-COR BioScience	Cat#926-32230
Corning Matrigel Growth Factor Reduced (GFR) Basement Membrane Matrix, Phenol Red-Free	Corning	Cat#356231
Stratagene Brilliant II SYBR Green QRT-PCR Master Mix	Agilent	Cat#600825
MTSEA biotin-XX	Biotium	Cat#90066
SPRI select reagent kit	Beckman Coulter	Cat#B23318
Agencourt AMPure XP	Beckman Coulter	Cat#A63881
NDiff Neuro-2 Medium Supplement (200X)	EMD Millipore	Cat#SCM012

Reagent or resource	Source	Identifier
Accutase	EMD Millipore	Cat#SCR005
LightCycler 480 SYBR Green I Master mix	Roche	Cat#0407516001
cOplete proteinase inhibitor cocktail	Roche	Cat#11697498001
Biotin-16-dUTP	Roche	Cat#11093070910
Lenti-X concentrator	Clontech	Cat#631232
Expand Long Template PCR kit	Roche	Cat#11681834001
DharmaFECT 4 Transfection Reagent	Dharmacon	Cat#T-2004
Cell Line Nucleofector Kit V	Lonza	Cat#VVCA-1003
TransIT LT1 Transfection Reagent	Mirus	Cat#MIR2300
HyClone fetal bovine serum	GE Healthcare	Cat#11995
Proteinase K	MacheryNagel	Cat#740506
Critical Commercial Assays		
TruSeq Stranded Total RNA LT - (with Ribo-Zero Human/Mouse/Rat)	Illumina	Cat#RS-122-2201
Nextera DNA Sample Preparation Kit	Illumina	Cat#Fc-121-1030
Cell proliferation kit (MTT)	Roche	Cat#11465007001
Luciferase reporter assay system	Promega	Cat#E1500
NEBNext Ultra II DNA Library Prep Kit for Illumina	NEB	Cat#E7645S
MycoAlert PLUS mycoplasma detection kit	Lonza	Cat#LT07-705
Deposited Data		
Raw and analyzed data of human cell line	this study	GEO: GSE97669
Raw and analyzed data of mouse cell line	this study, Xu et al., 2017	GEO: GSE84646, GSE97669
ICGC (release 23)	N/A	https://dcc.icgc.org/releases
METABRIC	Curtis et al., 2012	EGA:EGAD00001003342
Experimental Models: Cell Lines		
Human: MDA-MB-231 cell line	ATCC	HTB-26
Human: MDA-MB-231 CRISPRi clones	Liu et al., 2017	N/A
Human: MCF-7 cell line	ATCC	HTB-22
Human: MCF-7 CRISPRi clones	Liu et al., 2017	N/A
Human: HEK-293 cell line	ATCC	CRL-1573
Human: 293T cell line	ATCC	CRL-3216
Human: MCF10A cell line	ATCC	CRL-10317
Human: SKBR3 cell line	ATCC	HTB-30
Human: HCT116 cell line	ATCC	CCL-247
Human: HeLa cell line	ATCC	CCL-2
Mouse: neuronal progenitor cell line	Xu et al., 2017	N/A
Mouse: neuronal progenitor cell clones	Xu et al., 2017	N/A
Mouse: embryonic stem cell line	Xu et al., 2017	N/A
Mouse: embryonic stem cell line clones	Xu et al., 2017	N/A
Experimental Models: Organisms/Strains		

Reagent or resource	Source	Identifier
Mouse: NOD.*Cg-Prkdc*^{scid}*Il2rg*^{tm1Wjl}/SzJ	Jackson laboratories	Cat#005557
Oligonucleotides		
sgRNA sequences, see Table S1	this paper; Liu et al., 2017	N/A
ASO sequences, see Table S1	this paper	see Table S1
siRNA sequences, see Table S1	this paper; Tseng et al., 2014	see Table S1
qRT-PCR primers, see Table S1	this paper; Tseng et al., 2014	N/A
qPCR primers, see Table S1	this paper	N/A
primers used for northern blotting	this paper	N/A
primers used for plasmid cloning	this paper	N/A
primers used in UMI-4C library preparation, see Table S1	this paper	N/A
primers used in genotyping, see Table S1	this paper	N/A
primers used in targeted RNA-seq, see Table S1	this paper	N/A
Recombinant DNA		
pHR-SFFV-dCas9-BFP	Gilbert et al., 2014	Addgene#46910
pHR-SFFV-dCas9-BFP-KRAB	Gilbert et al., 2014	Addgene#46911
pHR-SFFV-dCas9-BFP-KRAB-2A-Blast	this paper	N/A
lenti-mU6-sgRNA-Puro-mCherry	this paper	N/A
lenti-mU6-sgRNA-Puro-EGFP	this paper	N/A
lenti-dCas9-VP64-2A-Blast	Konermann et al., 2015	Addgene#61425
lenti-MS2-P65-HSF1-Hygro	Konermann et al., 2015	Addgene#61426
lenti-sgRNA2.0-Puro-mCherry	this paper	N/A
lenti-EF1a-luciferase-2A-Hygro	this paper	N/A
pET-Cas9	this paper	N/A
pGL4.23[luc2/minP]	Promega	Cat#E8411
lenti-bovine U6 promoter-sgRNA, pMJ114	Adamson et al., 2016	Addgene#85995
lenti-human U6 promoter-sgRNA, pMJ117	Adamson et al., 2016	Addgene#85997
lenti-mouse U6 promoter-sgRNA, pMJ179	Adamson et al., 2016	Addgene#85996
Software and Algorithms		
LivingImagesoftware (v4.4)	Perkin Elmer	N/A
Image Studio (v1.0.11)	LI-COA BioScience	N/A
Tophat2 (v2.1.1)	Kim et al., 2013	http://ccb.jhu.edu/software/tophat/index.shtml
DEseq2 (v1.16.1)	Love et al., 2014	https://bioconductor.org/packages/release/bioc/html/DESeq2.html
Bowtie2 (v2.2.8)	Langmead and Salzberg, 2012	http://bowtie-bio.sourceforge.net/bowtie2/index.shtml
Picard (v.1.79)	N/A	http://broadinstitute.github.io/picard/
MACS2 (v2.1.0)	Zhang et al., 2008	https://github.com/taoliu/MACS
Samtools (v1.3.1)	Li et al., 2009	http://samtools.sourceforge.net
Bedtools (v2.17.0)	Quinlan and Hall, 2010	http://bedtools.readthedocs.io/en/latest/

Reagent or resource	Source	Identifier
HiC-pro (v.2.7.8)	Servant et al., 2015	https://github.com/nservant/HiC-Pro
Fastax-collapser (Fastx Toolkit v0.0.14)	N/A	http://hannonlab.cshl.edu/fastx_toolkit/
CADD	Kircher et al., 2014	http://cadd.gs.washington.edu/score
CRISPResso (v1.0.0)	Pinello et al., 2016	http://crispresso.rocks
HISAT2 (v2.0.1)	Kim et al., 2015	https://ccb.jhu.edu/software/hisat2/index.shtml
R Statistical Programming Language and Bioconductor	Gentleman et al., 2004	https://www.r-project.org
Other		